Big bang nucleosynthesis: Present status

Richard H. Cyburt

Joint Institute for Nuclear Astrophysics (JINA), National Superconducting Cyclotron Laboratory (NSCL), Michigan State University, East Lansing, Michigan 48824, USA

Brian D. Fields

Departments of Astronomy and of Physics, University of Illinois, Urbana, Illinois 61801, USA

Keith A. Olive

William I. Fine Theoretical Physics Institute, School of Physics and Astronomy, University of Minnesota, Minneapolis, Minnesota 55455, USA

Tsung-Han Yeh

Departments of Astronomy and of Physics, University of Illinois, Urbana, Illinois 61801, USA

(published 23 February 2016)

Big bang nucleosynthesis (BBN) describes the production of the lightest nuclides via a dynamic interplay among the four fundamental forces during the first seconds of cosmic time. A brief overview of the essentials of this physics is given, and new calculations presented of light-element abundances through ^{6}Li and ^{7}Li, with updated nuclear reactions and uncertainties including those in the neutron lifetime. Fits are provided for these results as a function of baryon density and of the number of neutrino flavors N_ν. Recent developments are reviewed in BBN, particularly new, precision *Planck* cosmic microwave background (CMB) measurements that now probe the baryon density, helium content, and the effective number of degrees of freedom $N_{\rm eff}$. These measurements allow for a tight test of BBN and cosmology using CMB data alone. Our likelihood analysis convolves the 2015 *Planck* data chains with our BBN output and observational data. Adding astronomical measurements of light elements strengthens the power of BBN. A new determination of the primordial helium abundance is included in our likelihood analysis. New D/H observations are now more precise than the corresponding theoretical predictions and are consistent with the standard model and the *Planck* baryon density. Moreover, D/H now provides a tight measurement of N_ν when combined with the CMB baryon density and provides a 2σ upper limit $N_\nu < 3.2$. The new precision of the CMB and D/H observations together leaves D/H predictions as the largest source of uncertainties. Future improvement in BBN calculations will therefore rely on improved nuclear cross-section data. In contrast with D/H and ^{4}He, ^{7}Li predictions continue to disagree with observations, perhaps pointing to new physics. This paper concludes with a look at future directions including key nuclear reactions, astronomical observations, and theoretical issues.

DOI: 10.1103/RevModPhys.88.015004

CONTENTS

I. INTRODUCTION

Big bang nucleosynthesis (BBN) is one of the few probes of the very early Universe with direct experimental or observational consequences (Walker *et al.*, 1991; Olive, Steigman, and Walker, 2000; Fields and Olive, 2006; Steigman, 2007; Iocco *et al.*, 2009; Fields, Molaro, and Sarkar, 2014). In the context of the standard models of cosmology and of nuclear and particle physics, BBN is an effectively parameter-free

theory (Cyburt, Fields, and Olive, 2002). Namely, standard BBN (SBBN) assumes spacetime characterized by general relativity and the Λ cold dark matter (ΛCDM) cosmology and microphysics characterized by standard model particle content and interactions, with three light neutrino species, with negligible effects due to dark matter and dark energy.

In SBBN, the abundances of the four light nuclei are usually parametrized by the baryon-to-photon ratio $\eta \equiv n_b/n_\gamma$, or equivalently the present baryon density $\Omega_b h^2 \equiv \omega_b$. This quantity has been fixed by a series of precise measurements of microwave background anisotropies, most recently by *Planck* yielding $\omega_b = 0.022\,25 \pm 0.000\,16$ or $\eta = 6.10 \pm 0.04$ (Ade *et al.*, 2015). Thus the success or failure of SBBN rests solely on the comparison of theoretical predictions with observational determinations.

While precise predictions from SBBN are feasible, they rely on well-measured cross sections and a well-measured neutron lifetime. Indeed, even prior to the WMAP era, theoretical predictions for D, ^{3}He, and ^{4}He were reasonably accurate; however, uncertainties in nuclear cross sections leading to ^{7}Be and ^{7}Li were relatively large. Several modern analyses of nuclear rates for BBN were based on the NACRE compilation (Angulo *et al.*, 1999) and recent BBN calculations [some using rate calculations with less ambiguous definitions of rate uncertainties (Cyburt, 2004; Descouvemont *et al.*, 2004; Serpico *et al.*, 2004)] by several groups are in good agreement (Nollett and Burles, 2000; Vangioni-Flam, Coc, and Casse, 2000; Burles, Nollett, and Turner, 2001; Cyburt, Fields, and Olive, 2001, 2003; Coc *et al.*, 2002, 2004, 2012; Cuoco *et al.*, 2004; Descouvemont *et al.*, 2004; Serpico *et al.*, 2004; Cyburt, 2004). Recent remeasurements of the $^3\mathrm{He}(\alpha,\gamma)^7\mathrm{Be}$ cross section (Singh *et al.*, 2004; Brown *et al.*, 2007; Confortola *et al.*, 2007; Gyürky *et al.*, 2007) did improve the theoretical accuracy of the prediction but exacerbated the discrepancy between theory and observation (Cyburt, Fields, and Olive, 2008). Very recently, the NACRE Collaboration issued an update (NACRE-II) of its nuclear rate tabulation (Xu *et al.*, 2013). These were first used by Coc, Uzan, and Vangioni (2014) and we incorporated the new rates in the results discussed later. NACRE-II is mainly useful in updating reactions to the network involving $A > 7$ nuclei.

The neutron mean life has had a rather sordid history. Because it scales the weak interaction rates between $n \leftrightarrow p$, the neutron mean life controls the neutron-to-proton ratio at freeze-out and directly affects the ^{4}He abundance (and the other light elements to a lesser extent). The value $\tau_n = 918 \pm 14$ s reported by Christensen *et al.* (1972) dominated the weighted mean for the accepted value through the mid-1980s. Despite the low value of 877 ± 8 s reported by Bondarenko *et al.* (1978), the "accepted" mean value (as reported in the Review of Particle Physics) remained high, and the high value was reinforced by a measurement by Byrne *et al.* (1980) of 937 ± 18 s. The range 877–937 s was used by Olive *et al.* (1981) to explore the sensitivity of BBN predictions to this apparently uncertain quantity treated then as an uncertain input parameter to BBN calculations (along with the number of light neutrino flavors N_ν and the baryon-to-photon ratio η). In the late 1980s a number of lower measurements began to surface, and Mampe *et al.* (1989) claimed to measure a mean life of 877.6 ± 3 s (remarkably consistent with the current world average). Subsequently, it appeared that questions regarding the neutron mean life had been resolved, as the mean value varied very little between 1990 and 2010, settling at 885.6 ± 0.8. However, in 2005, there was already a sign that the mean life was about to shift to lower values once again. Serebrov *et al.* (2005) reported a very precise measurement of 878.5 ± 0.8 which was used in BBN calculations by Mathews, Kajino, and Shima (2005). This was followed by several more recent measurements and reanalyses tending to lower values so that the current Particle Data Group world average is $\tau_n = 880.3 \pm 1.1$ (Olive *et al.*, 2014).

Note that this world average is dominated by experiments using the storage of ultracold neutrons in traps or bottles. However, experiments measuring τ_n by decay in flight in beams show significantly longer lifetimes of 887.7 ± 2.3 (Yue *et al.*, 2013). There is hope that new experiments will be able to resolve this discrepancy within the next few years (Bowman *et al.*, 2014). An accuracy of a few tenths of a second is needed to test the unitarity of the Cabibbo-Kobayashi-Maskawa (CKM) matrix at the level of 1 part in 10^{-4}. Here we assume the current world average and we explore the impact of the new lifetime on the light-element abundances.

On the observational side, the ^{4}He abundance determination comes most directly from measurements of emission lines in highly ionized gas in nearby low-metallicity dwarf galaxies (extragalactic HII regions). The helium abundance uncertainties are dominated by systematic effects (Olive and Skillman, 2001, 2004; Aver, Olive, and Skillman, 2010, 2011, 2012). The model used to determine the ^{4}He abundance contains eight physical parameters, including the ^{4}He abundance that is used to predict a set of ten H and He emission line ratios, which can be compared with observations (Izotov, Thuan, and Lipovetsky, 1994, 1997; Izotov, Thuan, and Stasińska, 2007; Izotov, Stasinska, and Guseva, 2013; Izotov, Thuan, and Guseva, 2014). Unfortunately, there are only a dozen or so observations for which the data and/or model are reliable, and even in those cases, degeneracies among the parameters often lead to relatively large uncertainties for each system as well as a large uncertainty in the regression to zero metallicity. Newly calculated ^{4}He emissivities (Porter *et al.*, 2012, 2013) and the addition of a new near infrared line (Izotov, Thuan, and Guseva, 2014) have led to lower abundance determinations (Aver *et al.*, 2013; Aver, Olive, and Skillman, 2015), bringing the central value of the ^{4}He abundance determination into good agreement with the SBBN prediction. Moreover, *Planck* measurements of cosmic microwave background (CMB) anisotropies are now precise enough to give interesting measures of primordial helium via its effect on the anisotropy damping tail.

New observations and analyses of quasar absorption systems have dramatically improved the observational determination of D/H. Using a handful of systems where accurate determinations can be made, Cooke *et al.* (2014) not only significantly lowered the uncertainty in the mean D/H abundance, but the dispersion present in old data has all but been erased. Because of its sensitivity to the baryon density, D/H is a powerful probe of SBBN and now the small uncertainties in both the data and prediction become an

excellent test of concordance between SBBN and the CMB determination of the baryon density.

In contrast to the predicted abundances of ^{4}He and D/H, the ^{7}Li abundance shows a definite discrepancy with all observational determinations from halo dwarf stars. To date, there is no solution that is either not tuned or requires substantial departures from standard model physics. Attempts at solutions include modifications of the nuclear rates (Cyburt, Fields, and Olive, 2004; Boyd *et al.*, 2010; Coc *et al.*, 2012) or the inclusion of new resonant interactions (Chakraborty, Fields, and Olive, 2011; Broggini *et al.*, 2012; Cyburt and Pospelov, 2012); stellar depletion (Pinsonneault *et al.*, 1999, 2002; Vauclair and Charbonnel, 1998; Richard, Michaud, and Richer, 2005; Korn *et al.*, 2006; García Peréz *et al.*, 2008); lithium diffusion in the postrecombination universe (Pospelov and Afshordi, 2012; Kusakabe and Kawasaki, 2015); new (nonstandard model) particles decaying around the time of BBN (Jedamzik, 2004a, 2004b; Kawasaki, Kohri, and Moroi, 2005a, 2005b; Jedamzik and Pospelov, 2009; Cyburt *et al.*, 2010, 2012, 2013; Pospelov and Pradler, 2010; Poulin and Serpico, 2015); axion cooling (Erken *et al.*, 2012; Kusakabe *et al.*, 2013); or variations in the fundamental constants (Dmitriev, Flambaum, and Webb, 2004; Coc *et al.*, 2007, 2012; Berengut, Flambaum, and Dmitriev, 2010).

In this review, we survey the current status of SBBN theory and its compatibility with observation. Using an up-to-date nuclear network, we present new Monte Carlo estimates of the theoretical predictions based on a full set of nuclear cross sections and their uncertainties. We highlight those reactions that still carry the greatest uncertainties and how those rates affect the light-element abundances. We also highlight the effect of the new determination of the neutron mean life on the ^{4}He abundance and the abundances of the other light elements as well.

Compatibility with observation is demonstrated by the construction of likelihood functions for each of the light elements (Cyburt, Fields, and Olive, 2001) by convolving individual theoretical and observational likelihood functions. Our BBN calculations are also convolved with data chains provided by the 2015 *Planck* data release (Ade *et al.*, 2015). This allows us to construct two-dimensional (η, Y_p) and three-dimensional (η, Y_p, N_ν) likelihood distributions. Such an analysis is timely and important given the recent advances in the ^{4}He and D/H observational landscape. In fact, despite the accuracy of the SBBN prediction for D/H, the small uncertainty in observed D/H now leads to a likelihood dominated by theory errors. The tight agreement between D/H prediction and observation is in sharp contrast to the discrepancy in ^{7}Li/H. We briefly discuss this "lithium problem," and discuss recent nuclear measurements that rule out a nuclear fix to this problem, leaving as explanations either astrophysical systematics or new physics. While the ^{6}Li was shown to be an artifact of astrophysical systematics (Cayrel *et al.*, 2007; Perez *et al.*, 2009; Steffen *et al.*, 2009; Lind *et al.*, 2013), for now the ^{7}Li problem persists.

As a tool for modern cosmology and astroparticle physics, SBBN is a powerful probe for constraining physics beyond the standard model (Sarkar, 1996; Cyburt *et al.*, 2005). Often these constraints can be parametrized by the effect of new physics on the speed-up of the expansion rate of the Universe and subsequently translated into a limit on the number of equivalent neutrino flavors or the effective number of relativistic degrees of freedom $N_{\rm eff}$. We update these constraints and compare them to recent limits on $N_{\rm eff}$ from the microwave background anisotropy and large scale structure. We show that for the first time D/H provides a more stringent constraint on $N_{\rm eff}$ than the ^{4}He mass fraction.

The structure of this review is as follows: In Sec. II we discuss the relevant updates to the nuclear rates used in the calculation of the light-element abundances. We also discuss the sensitivity to the neutron mean life. In this section, we present our baseline results for SBBN assuming the *Planck* value for η, the Particle Data Group world average for τ_n, and $N_\nu = 3$. In Sec. III we briefly review the values of the observational abundance determinations and their uncertainties that we adopt for comparison with the SBBN calculations from the previous section. In Sec. IV we discuss our Monte Carlo methods and construct likelihood functions for each of the light elements, and we extend these methods to discuss limits on N_ν in Sec. V. The lithium problem is summarized in Sec. VI. A discussion of these results and the future outlook appears in Sec. VII.

II. PRELIMINARIES

A. SBBN

As defined in Sec. I, SBBN refers to BBN in the context of Einstein gravity, with a Friedmann-Lemaître-Robertson-Walker cosmological background. It assumes the standard model of nuclear and particle physics, or, in other words, the standard set of nuclear and particle interactions and nuclear and particle content. Implicitly, this means a theory with a number $N_\nu = 3$ of very light neutrino flavors.[1] SBBN also makes the well-justified assumption that during the epoch of nucleosynthesis the Universe was radiation dominated, so that the dominant component of the energy density of the Universe can be expressed as

$$\rho = \frac{\pi^2}{30}\left(2 + \frac{7}{2} + \frac{7}{4}N_\nu\right)T^4, \tag{1}$$

taking into account the contributions of photons, electrons, and positrons, and neutrino flavors appropriate for temperatures $T > 1$ MeV. At these temperatures, weak interaction rates between neutrons and protons maintain equilibrium.

At lower temperatures, the weak interactions can no longer keep up with the expansion of the Universe or, equivalently, the mean time for an interaction becomes longer than the age of the Universe. Thus, the freeze-out condition is set by

$$G_F^2 T^5 \sim \Gamma_{\rm wk}(T_f) = H(T_f) \sim G_N^{1/2} T^2, \tag{2}$$

[1]We distinguish between the number of neutrino flavors, three in the standard model, and $N_{\rm eff}$, equal to 3.046 in the standard model, which corresponds to the effective number of neutrinos present in the thermal bath due to the higher temperature from e^+e^- annihilations before neutrinos are completely decoupled.

where $\Gamma_{\rm wk}$ represents the relevant weak interaction rates per baryon that scale roughly as T^5, and H is the Hubble parameter

$$H^2 = \frac{8\pi}{3} G_N \rho \tag{3}$$

and scales as T^2 in a radiation dominated universe. G_F and G_N are the Fermi and Newton constants, respectively. Freeze-out occurs when the weak interaction rate falls below the expansion rate $\Gamma_{\rm wk} < H$. The β interactions that control the relative abundances of neutrons and protons freeze out at $T_f \sim 0.8$ MeV. At freeze-out, the neutron-to-proton ratio is given by the Boltzmann factor $(n/p)_f \simeq e^{-\Delta m/T_f} \sim 1/5$, where $\Delta m = m_n - m_p$ is the neutron-proton mass difference. After freeze-out, free neutron decays drop the ratio slightly to $(n/p)_{\rm bbn} \simeq 1/7$ before nucleosynthesis begins. A useful semi-analytic description of freeze-out can be found in Bernstein, Brown, and Feinberg (1989) and Mukhanov (2004).

The first link in the nucleosynthetic chain is $p + n \to d + \gamma$ and although the binding energy of deuterium is relatively small, $E_B = 2.2$ MeV, the large number of photons relative to nucleons $\eta^{-1} \sim 10^9$ causes the so-called deuterium bottleneck. BBN is delayed until $\eta^{-1} \exp(-E_B/T) \sim 1$ when the deuterium destruction rate finally falls below its production rate. This occurs when the temperature is $T \sim E_B/\ln\eta^{-1} \sim 0.1$ MeV.

To a good approximation, almost all of the neutrons present when the deuterium bottleneck breaks end up in ^{4}He. It is therefore easy to estimate the ^{4}He mass fraction,

$$Y_p = \frac{2(n/p)}{1 + (n/p)} \approx 0.25, \tag{4}$$

where we evaluated Y_p using $(n/p) \approx 1/7$. The other light elements are produced in significantly smaller abundances, justifying our approximation for the ^{4}He mass fraction. D and ^{3}He are produced at the level of about 10^{-5} by number, and ^{7}Li at the level of 10^{-10} by number. A cooling universe, Coulomb barriers, and the mass gap at $A = 8$ prevents the production of other isotopes in any significant quantity. For more on the physics of BBN, see Bernstein, Brown, and Feinberg (1989), Mukhanov (2004, 2005), Weinberg (2008), and Iocco *et al.* (2009).

B. Updated nuclear rates

Our BBN results use an updated version of our code (Cyburt, Fields, and Olive, 2001, 2008), itself a descendant of the Wagoner code (Wagoner, 1969). For the weak $n \leftrightarrow p$ interconversion rates, the code calculates the 1D phase space integrals at tree level; this corresponds to the assumption that the nucleon remains at rest. The weak $n \leftrightarrow p$ interconversion rates are normalized such that we recover the adopted mean neutron lifetime at low temperature and density. To this we added order-α radiative and bremsstrahlung quantum electrodynamics (QED) corrections and included Coulomb corrections for reactions with pe^- in the initial or final states (Dicus *et al.*, 1982; Smith and Fuller, 2010). We neglected additional corrections, because the overall contribution of all other effects is relatively insignificant. Finite temperature radiative corrections lead to $\Delta Y_p \sim 0.0004$, corrections to electron mass lead to $\Delta Y_p \sim -0.0001$, and neutrino heating due to e^+e^- annihilation leads to $\Delta Y_p \sim 0.0002$ (Dicus *et al.*, 1982; Smith and Fuller, 2010). Problems in the original code due to the choice of time steps in the numerical integration (Kernan, 1993) have been corrected here. Finally, we included the effects of finite nucleon mass (Seckel, 1993; Lopez, Turner, and Gyuk, 1997) by increasing the final ^{4}He abundance with $\Delta Y_p = +0.0012$. We formally adopt the Particle Data Group's current recommended value (Olive *et al.*, 2014): $\tau_n = 880.3 \pm 1.1$ for the mean free neutron decay lifetime and assume it is normally distributed.

TABLE I. Reactions of relevance for BBN from the NACRE-II compilation.

$d(p,\gamma)^3$He	$d(d,\gamma)^4$He	$d(d,n)^3$He
$d(d,p)t$	$t(d,n)^4$He	^{3}He$(d,p)^4$He
$d(\alpha,\gamma)^6$Li	^{6}Li$(p,\gamma)^7$Be	^{6}Li$(p,\alpha)^3$He
^{7}Li$(p,\alpha)^4$He	^{7}Li$(p,\gamma)^8$Be[a]	

[a] ^{8}Be is not in our nuclear network; ^{8}Be is assumed to spontaneously decay into 2^4He.

In addition to the weak $n \leftrightarrow p$ interconversion rates, BBN relies on well-measured cross sections. The latest update to these reaction rates was evaluated by the NACRE Collaboration and released as NACRE-II (Xu *et al.*, 2013). Only charge-induced reactions were considered in NACRE-II, and many more reactions are evaluated there than is relevant for BBN. Those reactions of relevance are shown in Table I. The error analysis of the rates by the first NACRE compilation was not done in a strict statistical way. This problem was treated at length by Cyburt, Fields, and Olive (2001), where a detailed comparison of the NACRE theoretical S-factor fits to the data sets they use was made. To assess the uncertainties in the cross sections, we used a χ^2 analysis to describe the goodness of fit of the theory to the data, given the experimental errors. Unfortunately the NACRE rates are not always fit to the energy range needed for BBN, and as a consequence, it was necessary to go back to the data and renormalize the S-factor fits.

The NACRE-II compliation improves upon NACRE not only in adding new experimental data, but also by adopting physically motivated cross-section fits. These fits were based on potential models described by a handful of parameters, which allowed for the systematic study of the uncertainties in the models. The compilation presents tables of reaction rates, with recommended "adopted," "low," and "high" values. NACRE describe the high and low rates as "lower and upper limits" to the adopted rates, but do not present them as statistically defined limits, such as 1σ or 2σ ranges. We assume the rates are distributed with a log-normal distribution with

$$\mu \equiv \ln \sqrt{R_{\rm high} R_{\rm low}}, \tag{5}$$

$$\sigma \equiv \ln \sqrt{R_{\rm high}/R_{\rm low}}, \tag{6}$$

TABLE II. Comparison of BBN results.

Reference	η_{10}	N_ν	Y_p	D/H	^{3}He/H	^{7}Li/H	^{6}Li/H
This work	6.10	3	0.2470	2.579×10^{-5}	0.9996×10^{-5}	4.648×10^{-10}	1.288×10^{-14}
Iocco *et al.* (2009) fit	6.10	3	0.2463	2.578×10^{-5}	0.9983×10^{-5}	4.646×10^{-10}	1.290×10^{-14}

where $R_{\rm low}$ and $R_{\rm high}$ are the recommended low and high values for the reaction rates, respectively (Coc, Uzan, and Vangioni, 2014). These rates agree well with previous evaluations (Cyburt, Fields, and Olive, 2001; Cuoco *et al.*, 2004; Cyburt, 2004; Descouvemont *et al.*, 2004), largely because they depend on the same experimental data. Uncertainties in the NACRE-II evaluation are similar to but tend to be larger than previous studies. This may stem from the method used to derive accurate descriptions of the data and the fitting potential models used in distorted-wave Born approximation calculations.

The remaining relevant n-induced rates $p(n,\gamma)d$, ^{3}He$(n,p)t$, and ^{7}Be$(n,p)^7$Li, need to be taken from different sources. We adopt the evaluation from Ando *et al.* (2006) for the key reaction $p(n,\gamma)d$. The remaining (n,p) reactions we use are rates taken from Cyburt (2004). Finally we took ^{3}He$(\alpha,\gamma)^7$Be from Cyburt and Davids (2008) and $t(\alpha,\gamma)^7$Li from Cyburt (2004). We choose log-normal parameters in such a way to keep the means and variances of the reaction rates invariant. We note that in the code used here, the network extends isotopes through Al. A dedicated analysis of $A > 7$ isotopes was treated in Iocco *et al.* (2007), Coc *et al.* (2012), and Coc, Uzan, and Vangioni (2014).

C. First results

As a prelude to the more detailed analysis given next, we first discuss the BBN predictions at a fixed value of η. This benchmark can then be compared to the results of other codes.

Here we fix $\eta_{10} \equiv 10^{10}\eta = 6.10$. This is related to the value of ω_b determined by *Planck* (Ade *et al.*, 2015) based on a combination of temperature and polarization data.[2] The result of our BBN calculation at $\eta_{10} = 6.10$ can be found in Table II compared to the fit in Iocco *et al.* (2009), based on the PArthENoPE code (Pisanti *et al.*, 2008). As one can see, the results of the two codes are in excellent agreement for all of the light elements. While the rates used are very similar, they are not exactly the same between the two codes. The results can be quickly compared with the observed abundances given in Sec. III. However a more rigorous treatment of the comparison between theory and observation is given in Sec. IV.

III. OBSERVATIONS

Before making a direct comparison of the SBBN results, we first discuss astrophysical observations of light elements. Here we focus on ^{4}He, D, and the Li isotopes, all of which are accessible in primitive environments making it possible to extrapolate existing observations to their primordial abundances. BBN also produces ^{3}He in observable amounts, and ^{3}He is detectable via its hyperfine emission line, but this line is accessible only within Milky Way gas clouds that are far from pristine (Rood, Wilson, and Steigman, 1979). Because of the uncertain post-BBN nucleosynthetic history of ^{3}He, it is not possible to use these high-metallicity environments to infer primordial ^{3}He at a level useful for probing BBN (Galli *et al.*, 1995, 1997; Olive *et al.*, 1995, 1997; Dearborn, Steigman, and Tosi, 1996; Scully *et al.*, 1996, 1997; Bania, Rood, and Bania, 2002; Vangioni-Flam *et al.*, 2003). After an overview of the observational status of the four remaining isotopes, we turn to the CMB, which includes constraints not only on the baryon density but now also on ^{4}He and $N_{\rm eff}$.

A. Helium-4

^{4}He has long since been the element of choice for setting constraints on physics beyond the standard model. The reasoning is simple: as discussed previously, the ^{4}He abundance is almost completely controlled by the number of free neutrons at the onset of nucleosynthesis, and that number is determined by the freeze-out of the weak $n \leftrightarrow p$ rates. The resulting mass fraction of ^{4}He is given in Eq. (4). As seen, the SBBN result for the Y_p dependence on the baryon density is only logarithmic and therefore ^{4}He is not a particularly good baryometer. Nevertheless, it is quite sensitive to any changes in the freeze-out temperature T_f, through Eq. (2). However, strong limits on physics beyond the standard model (Sarkar, 1996; Cyburt *et al.*, 2005) require accurate ^{4}He abundances from observations.

The ^{4}He abundance is determined by measurements of He (and H) emission lines in extragalactic H II regions. Since ^{4}He is produced in stars along with heavier elements, the primordial mass fraction of ^{4}He $Y_p \equiv \rho(^4\text{He})/\rho_b$ is determined by a regression of the helium abundance versus metallicity (Peimbert and Torres-Peimbert, 1974). However, due to numerous systematic uncertainties, obtaining an accuracy better than 1% in the primordial helium abundance is very difficult (Olive and Skillman, 2001, 2004; Izotov, Thuan, and Stasińska, 2007; Peimbert, Luridiana, and Peimbert, 2007). The theoretical model that is used to extract a ^{4}He abundance contains eight physical parameters to predict the fluxes of nine emission line ratios that can be compared directly with observations.[3] The parameters include the electron density, optical depth, temperature, equivalent widths of underlying absorption for both H and He, a correction for reddening, the neutral hydrogen fraction, and of course the ^{4}He abundance.

[2] A straight interpretation of the *Planck* result based on the $TT, TE, EE, +\text{low}P$ anisotropy data would yield $\eta_{10} = 6.09$. However, this result already includes the He abundance from BBN. Our choice of η is discussed in Sec. IV.C and Table IV.

[3] Later we use results based on the inclusion of a tenth line (seventh He line) seen in the near infrared (Izotov, Thuan, and Guseva, 2014).

Using theoretical emissivities, the model can be used to predict the fluxes of six He lines (relative to Hβ) as well as three H lines (also relative to Hβ). The lines are chosen for their ability to break degeneracies among the inputs when possible. For a recent discussion, see Aver *et al.* (2013) and Aver, Olive, and Skillman (2015).

There is a considerable amount of ^{4}He data available (Izotov, Thuan, and Lipovetsky, 1994, 1997; Izotov, Thuan, and Stasińska, 2007). A Markov chain Monte Carlo (MCMC) analysis of the eight-dimensional parameter space for 93 H II regions reported in Izotov, Thuan, and Stasińska (2007) was performed in Aver, Olive, and Skillman (2012). By marginalizing over the other seven parameters, the ^{4}He abundance (and its uncertainty) can be determined. However, for most of the data, the χ^2's obtained by comparing the theoretically derived fluxes for the nine emission lines with those observed were typically very large ($\gg 1$) indicating either a problem with the data, a problem with the model, or problems with both. Selecting only data for which six He lines were available, and a $\chi^2 < 4$, left only 25 objects for the subsequent analysis. Further cuts of solutions with, for example, anomalously high neutral H fractions or excessive corrections due to underlying absorptions brought the sample down to 14 objects that yielded $Y = 0.2534 \pm 0.0083 + (54 \pm 102)\mathrm{O/H}$ based on a linear regression and $Y_p = 0.2574 \pm 0.0036$ based on a weighted mean of the same data.

Recently, a new analysis of the theoretical emissivities was performed (Porter *et al.*, 2012, 2013). This includes improved photoionization cross sections and a correction of errors found in the previous result. The new emissivities are systematically higher, and for some lines the increase in the emissivity is 3%–5% or higher. As a consequence, one expects lower ^{4}He abundances using the new emissivities. Aver *et al.* (2013) used the same initial data with the same quality cuts, now leaving 16 objects in the final sample. Individual objects typically showed 5%–10% lower ^{4}He abundance yielding $Y = 0.2465 \pm 0.0097 + (96 \pm 122)\mathrm{O/H}$ for a regression. Once again, one could argue that the lack of true indication of a slope in the data over the restricted baseline may justify using the mean rather than the regression. The mean was then found to be $Y_p = 0.2535 \pm 0.0036$. The large errors in Y_p determined from the regression were due to a combination of large errors on individual objects, a relatively low number of objects with $\chi^2 < 4$, a short baseline in O/H, and a poorly determined slope (although the analysis using the new emissivities shows more positive evidence for a slope of Y vs O/H).

More recently, new observations include a near infrared line at λ10830 (Izotov, Thuan, and Guseva, 2014). The importance of this line stems from its dependence on density and temperature that differs from other observed He lines. This potentially breaks the degeneracy seen between these two parameters that is one of the major culprits for large uncertainties in ^{4}He abundance determinations. There are 16 objects satisfying $\chi^2 \lesssim 6$ (Aver, Olive, and Skillman, 2015) (there are now 2 degrees of freedom rather than 1), with all seven He measured [although these are not exactly the same 16 objects used by Aver *et al.* (2013)]. Indeed it was found (Aver, Olive, and Skillman, 2015) that the inclusion of this line did in fact reduce the uncertainty and lead to a better defined regression

$$Y_p = 0.2449 \pm 0.0040 + (78.9 \pm 43.3)\mathrm{O/H}. \quad (7)$$

Unlike past analyses, there is now a well-defined slope in the regression, making the mean $Y_p = 0.2515 \pm 0.0017$ less justifiable as an estimate of primordial ^{4}He. The benefit of adding the IR He line is seen to reduce the uncertainty in Y_p by over a factor of 2. This is due to the better determined abundances of individual objects and a better determined slope. Even with the inclusion of the additional line, most of the available observational data are not well fitted by the model.

A higher value of $Y_p = 0.2551 \pm 0.0022$ was found by Izotov, Thuan, and Guseva (2014). A more detailed discussion of the differences between this result and the one given in Eq. (7) can be found in Aver, Olive, and Skillman (2015). We note here that the difference lies in how the helium abundance in individual objects is determined and by the sample selection. As discussed previously, much of the data are poorly described by the model and should not be used in a further statistical analysis to determine Y_p and, although the values of Y in individual objects are generally within 1σ between the two analyses, the MCMC methods used by Aver, Olive, and Skillman (2012, 2015) and Aver *et al.* (2013) generally result in uncertainties a factor of 2 times larger than those quoted by Izotov, Thuan, and Guseva (2014). Comparing with the value of Y_p given in Table II, the intercept of the regression (7) is in good agreement with the results of SBBN.

B. Deuterium

Because of its strong dependence on the baryon density, deuterium is an excellent baryometer. Furthermore, since there are no known astrophysical sources for deuterium production (Epstein, Lattimer, and Schramm, 1976; Prodanović and Fields, 2003) and thus all deuterium must be of primordial origin, any observed deuterium provides us with an upper bound on the baryon-to-photon ratio (Reeves *et al.*, 1973; Gott *et al.*, 1974). However, the monotonic decrease in the deuterium abundance over time indicates that the galactic chemical evolution (Audouze and Tinsley, 1974; Ostriker and Tinsley, 1975; Vangioni-Flam and Audouze, 1988; Steigman and Tosi, 1992; Edmunds, 1994; Vangioni-Flam, Olive, and Prantzos, 1994; Fields, 1996; Scully *et al.*, 1997; Casse *et al.*, 1998; Tosi *et al.*, 1998; Fields *et al.*, 2001; Steigman, Romano, and Tosi, 2007; Vangioni *et al.*, 2011; Olive *et al.*, 2012) affects the interpretation of any local measurements of the deuterium abundance such as in the local interstellar medium (Moos *et al.*, 2002; Linsky, 2003; Wood *et al.*, 2004; Prodanović, Steigman, and Fields, 2010), galactic disk (Linsky *et al.*, 2006), or galactic halo (Savage *et al.*, 2007).

The role of D/H in BBN was significantly promoted when measurements of D/H ratios in quasar absorption systems at high redshift became available. In a short note, Adams (1976) outlined the conditions that would permit the detectability of deuterium in such systems. However, it was not until 1997 that the first reliable measurements of D/H at high redshift became available (Burles and Tytler, 1998a, 1998b) (we do not discuss here the tumultuous period with conflicting high and low measures of D/H). Over the next 20+ years, only a handful of new observations became available with abundances in the range $\mathrm{D/H} = (1\text{–}4) \times 10^{-5}$ (Burles and Tytler, 1998a, 1998b;

O'Meara *et al.*, 2001, 2006; Pettini and Bowen, 2001; Levshakov *et al.*, 2002; Kirkman *et al.*, 2003; Pettini *et al.*, 2008; Srianand *et al.*, 2010; Fumagalli, O'Meara, and Prochaska, 2011; Noterdaeme *et al.*, 2012). Despite the fact that there was considerable dispersion in the data (unexpected if these observations correspond to primordial D/H), the weighted mean of the data gave $\mathrm{D/H} = (3.01 \pm 0.21) \times 10^{-5}$ with a sample variance of 0.68. While the data were in reasonably good agreement with the SBBN predicted value (discussed in detail later) using the CMB-determined value for the baryon-to-photon ratio, the dispersion indicated that either the quoted error bars were underestimated and larger systematic errors were unaccounted for or if the dispersion was real, *in situ* destruction of deuterium must have taken place within these absorbers. In the latter case, the highest ratio ($\sim 4 \times 10^{-5}$) should be taken as the post-BBN value, leaving room for some post-BBN production of D/H that may have accompanied the destruction of ^{7}Li; we return to this possibility (or lack thereof) later.

Pettini and Cooke (2012) published results from a new observation of an absorber at $z = 3.05$ with $\mathrm{D/H} = (2.54 \pm 0.05) \times 10^{-5}$ corresponding to an uncertainty of about 2% that can be compared with typical uncertainties of 10%–20% in previous observations. This was followed by another precision observation and a reanalysis of the 2012 data along with a reanalysis of a selection of three other objects from the literature (chosen using a strict set of restrictions to be able to argue for the desired accuracy) (Cooke *et al.*, 2014). The resulting set of five absorbers yielded

$$\left(\frac{\mathrm{D}}{\mathrm{H}}\right)_p = (2.53 \pm 0.04) \times 10^{-5} \tag{8}$$

with a sample variance of only 0.05. We use this value in our SBBN analysis.[4]

C. Lithium

Lithium has by far the smallest observable primordial abundance in SBBN, but as we see provides an important consistency check on the theory—a check that currently is not satisfied. In SBBN, mass 7 is made in the form of stable ^{7}Li, but also as radioactive ^{7}Be. In its neutral form, ^{7}Be decays via electron capture with a half-life of 53 days. In the early Universe, however, the decay is delayed until the Universe is cool enough that ^{7}Be can finally capture an electron at $z \sim 30\,000$ (Khatri and Sunyaev, 2011), shortly before hydrogen recombination. Thus ^{7}Be decays long after the $\sim$3 min time scale of BBN, yet after recombination, all mass 7 takes the form of ^{7}Li. Consequently, ^{7}Li/H theory predictions sum both mass-7 isotopes. Note also that ^{7}Li production dominates at low η, while ^{7}Be dominates at high η, leading to the characteristic "lithium dip" versus baryon density in the Schramm plot (Fig. 1) described later.

[4]Note that the most recent measurement described by Reimer-Sørensen *et al.* (2015) has a somewhat larger uncertainty, and its inclusion does not affect the weighted mean in Eq. (8).

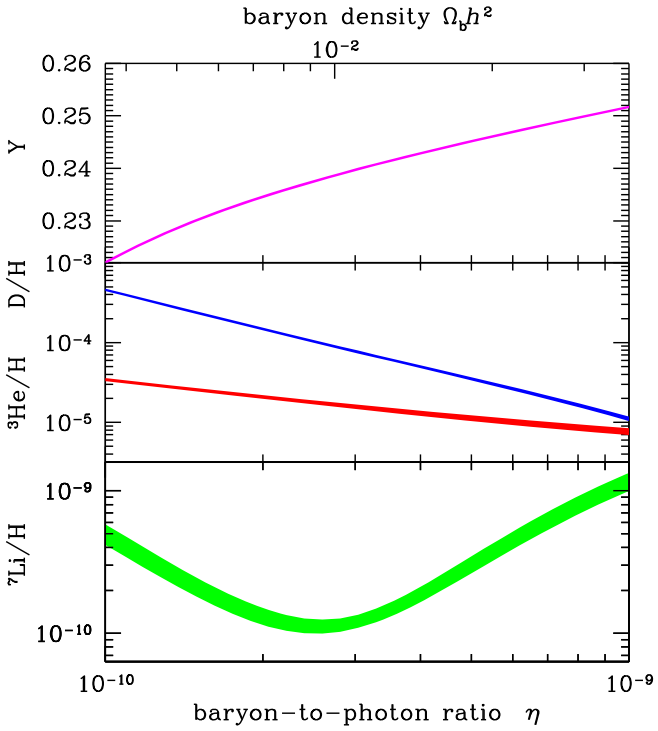

FIG. 1. Primordial abundances of the light nuclides as a function of cosmic baryon content as predicted by SBBN (the "Schramm plot"). These results assume $N_\nu = 3$ and the current measurement of the neutron lifetime $\tau_n = 880.3 \pm 1.1$ s. Curve widths show $1 - \sigma$ errors.

A wide variety of astrophysical processes have been proposed as lithium nucleosynthesis sites operating after BBN. Cosmic-ray interactions with diffuse interstellar (or intergalactic) gas produce both ^{7}Li and ^{6}Li via spallation reaction such as $p_{\mathrm{cr}} + {}^{16}\mathrm{O}_{\mathrm{ism}} \rightarrow {}^{6,7}\mathrm{Li} + \cdots$, and fusion ${}^4\mathrm{He}_{\mathrm{cr}} + {}^4\mathrm{He}_{\mathrm{ism}} \rightarrow {}^{6,7}\mathrm{Li} + \cdots$ (Reeves, Fowler, and Hoyle, 1970; Meneguzzi, Audouze, and Reeves, 1971; Prantzos, Cassé, and Vangioni-Flam, 1993; Ramaty *et al.*, 1997; Fields and Olive, 1999a; Rollinde, Vangioni-Flam, and Olive, 2005). In the supernova "ν process," neutrino spallation reactions can also produce ^{7}Li in the helium shell via $\nu + {}^4\mathrm{He} \rightarrow {}^3\mathrm{He}$ followed by ${}^3\mathrm{He} + {}^4\mathrm{He} \rightarrow {}^7\mathrm{Be} + \gamma$ as well as the mirror version of these (Woosley *et al.*, 1990; Heger *et al.*, 2005) although the importance of this contribution to ^{7}Li is limited by associated ^{11}B production (Olive *et al.*, 1994). Finally, in somewhat lower mass stars undergoing the late, asymptotic giant branch phase of evolution, ^{3}He burning leads to high surface Li abundances, some of that may (or may not) survive to be ejected in the death of the stars (Cameron and Fowler, 1971). Nova produced ^{7}Li may also contribute to its chemical evolution (Izzo *et al.*, 2015; Tajitsu *et al.*, 2015). Thus, despite its low abundance, ^{7}Li is the only element with significant production in the big bang, stars, and cosmic rays; by contrast, the only conventional site of ^{6}Li production is in cosmic-ray interactions (Reeves *et al.*, 1973; Fields and Olive, 1999b; Vangioni-Flam *et al.*, 1999).

To disentangle the diverse Li production processes observationally thus requires measurements of lithium abundances

as a function of metallicity. As with ^{4}He, the lowest-metallicity data should have a negligible Galactic contribution and point to the primordial abundances. To date, the only systems for which such a metallicity evolution can be traced are in metal-poor (population II) halo stars in our own Galaxy. As shown by Spite and Spite (1982), halo main sequence (dwarf or subgiant) stars with temperatures $T_{\rm eff} \gtrsim 6000$ K have a constant Li abundance, while Li/H decreases markedly for cooler stars. The hotter stars have thin convection zones and so Li is not brought to regions hot enough to destroy it. These hot halo stars that seem to preserve their Li are thus of great cosmological interest. Spite and Spite (1982) found that these stars with $[{\rm Fe/H}] \equiv \log[({\rm Fe/H})/({\rm Fe/H})_\odot] \lesssim -1.5$ have a substantially lower Li content than solar metallicity stars, and moreover the Li abundance does not vary with metallicity. This "Spite plateau" points to the primordial origin of Li. Furthermore, the Li/H abundance at the plateau gives the primordial value if the host stars have not destroyed any of their lithium.

The 1982 Spite plateau discovery was based on 11 stars in the plateau region. Since then, the number of stars on the plateau have increased by more than an order of magnitude. Increasingly precise observations showed that the scatter in Li abundances is very small for halo stars with metallicities down to $[{\rm Fe/H}] \sim -3$ (Molaro, Primas, and Bonifacio, 1995; Bonifacio and Molaro, 1997; Ryan, Norris, and Beers, 1999; Ryan *et al.*, 2000; Melendez and Ramirez, 2004; Bonifacio *et al.*, 2007; Hosford *et al.*, 2009, 2010).

Note, however, that a handful of stars in this metallicitiy range seem to have Li abundances outside above the observed plateau value. For example, Li/H lies about a factor of $\sim$2 above the plateau value in BD + 23 3912, a star at the upper edge of the plateau metallicity (King, Deliyannis, and Boesgaard, 1996). Objects such as these have received much attention in studies of stellar Li depletion via diffusion and/or mixing processes (Pinsonneault *et al.*, 1999, 2002; Vauclair and Charbonnel, 1998; Richard, Michaud, and Richer, 2005; Korn *et al.*, 2006; García Peréz *et al.*, 2008).

Recently, thanks to large increases in the numbers of known metal-poor halo stars, Li data have been extended to very low metallicity. Surprisingly, at metallicities below about $[{\rm Fe/H}] \lesssim -3$, the Li/H scatter becomes large, in contrast to the small scatter in the Spite plateau found at slightly higher metallicity. In particular, the trend in extremely metal-poor stars is that no stars have Li/H above the Spite plateau value, a few are found near the plateau, but many lie significantly below (Aoki *et al.*, 2009; Sbordone *et al.*, 2010; Frebel and Norris, 2015). This "meltdown" of the Spite plateau remains difficult to understand from the point of view of stellar evolution, but in any case seems to demand that at least some halo stars have destroyed their Li. Moreover, as seen later, this possibility has important consequences for the primordial lithium problem.

While the low-metallicity Li/H behavior is not understood, the Spite plateau remains at $[{\rm Fe/H}] \simeq -3$ to -1.5; lacking a clear reason to discard these data, we use them as a measure of primordial Li. Following Sbordone *et al.* (2010) we adopted their average of the nonmeltdown halo stars having $[{\rm Fe/H}] \gtrsim -3$, giving

$$\left(\frac{\rm Li}{\rm H}\right)_p = (1.6 \pm 0.3) \times 10^{-10}. \quad (9)$$

The stars in this sample were observed and analyzed in a uniform way, with Li abundances having been inferred from the absorption line spectra using sophisticated 3D stellar atmosphere models that do not assume local thermodynamic equilibrium (LTE).

Most halo star observations measure only elemental Li, because thermal broadening in the stellar atmospheres exceeds the isotope separation between ^{7}Li and ^{6}Li. However, very high signal-to-noise measurements are sensitive to asymmetries in the λ6707 line shape that encodes this isotope information. There were recent claims of ^{6}Li detections, with isotope ratios as high as $^6{\rm Li}/^7{\rm Li} \lesssim 0.1$ (Asplund *et al.*, 2006). The implied ^{6}Li/H abundance lies far above the SBBN value, leading to a putative "^{6}Li problem."

However, in recent analyses with 3D, non-LTE stellar atmosphere models included surface convection effects (akin to solar granulation) and showed that these can entirely explain the observed line asymmetry (Cayrel *et al.*, 2007; Perez *et al.*, 2009; Steffen *et al.*, 2009; Lind *et al.*, 2013). Thus the case for ^{6}Li detection in halo stars and for a ^{6}Li problem is weakened. Rather, the highest claimed $^6{\rm Li}/^7{\rm Li}$ ratio is best interpreted as an upper limit.

D. The cosmic microwave background

The CMB provides us with a snapshot of the Universe at recombination ($z_{\rm rec} \simeq 1100$) and encodes a wealth of cosmological information at unprecedented precision. In particular, the CMB provides a particularly robust, precise measure of the cosmic baryon content in a manner completely independent of BBN (Ade *et al.*, 2014, 2015; Spergel *et al.*, 2003; Hinshaw *et al.*, 2013; Komatsu *et al.*, 2014). Recently, the CMB determinations of $N_{\rm eff}$ and Y_p have also become quite interesting. In this section we see how the precision of the CMB has changed the role of BBN in cosmology and enhanced the leverage of BBN to probe new physics.

The physics of the CMB, and its relation to cosmological parameters, is recounted in excellent reviews such as White, Scott, and Silk (1994) and Hu and Dodelson (2002). Here we briefly and qualitatively summarize some of the key physics of the recombination epoch ($z_{\rm rec} \simeq 1100$) when the CMB was released.

Tiny primordial density fluctuations are laid down in the very early Universe, by inflation or some other mechanism. After matter-radiation equality $z_{\rm eq} \simeq 3400$, the dark matter density fluctuations grow and form increasingly deep gravitational potentials. The baryon-electron plasma is attracted to the potential wells and undergoes adiabatic compression as it falls in. Prior to recombination, the plasma remains tightly coupled to the CMB photons, whose pressure $P_\gamma \propto T^4$ acting as a restoring force, with sound speed $c_s^2 \sim 1/3$. This interplay of forces leads to acoustic oscillations of the plasma. The oscillations continue until (re)combination, when the Universe goes from an opaque plasma to a transparent gas of neutral H and He. The decoupled photons for the most part travel freely thereafter until detection today, recording a snapshot of the recombining Universe.

Because the density fluctuations are small, perturbations in the cosmic fluids are well described by linear theory, wherein different wave numbers evolve independently. Modes that have just attained their first contraction to a density maximum at recombination occur at the sound horizon $\sim c_s t_{\rm rec}$. This length scale projects onto the sky to a characteristic angular scale $\sim 1°$; this corresponds to the first and strongest peak in the CMB angular power spectrum. Higher harmonics correspond to modes at other density extrema. The acoustic oscillations depend on the cosmology as well as the plasma properties, which set the angular scales of the harmonics as well as the heights of the features, as well as the correspondence between the temperature anisotropies and the polarization. This gives rise to the CMB sensitivity to cosmological parameters.

Precision observations of CMB temperature and polarization fluctuations over a wide range of scales now exist and probe a host of cosmological parameters. Fortunately for BBN, one of the most robust of these is the cosmic baryon content, usually quantified in the CMB literature via the plasma (baryon + electron) density $\rho_{\rm b}$ written as the density parameter $\Omega_{\rm b} \equiv \rho_{\rm b}/\rho_{\rm crit}$, where the critical density $\rho_{\rm crit} = 3H_0^2/8\pi G$, with $H_0 = 100h$ km s^{-1} Mpc^{-1}, the present Hubble parameter. This in turn is related to the baryon-to-photon ratio η via

$$\eta = \frac{\rho_{\rm crit}}{\langle m \rangle n_\gamma^0} \Omega_B, \tag{10}$$

where $n_\gamma^0 = 2\zeta(3)T_0^3/\pi^2$ is the present-day equilibrium photon number density [$\zeta(3) \approx 1.202$ is the Riemann-zeta function]. The mean mass per baryon $\langle m \rangle$ in Eq. (10) is roughly the proton mass, but slightly lower due to the binding energy of helium. As a result, the detailed conversion depends very mildly on the ^{4}He abundance (Steigman, 2006), and we have

$$\eta_{10} = 273.3036 \Omega_B h^2 (1 + 7.169\,58 \times 10^{-3} Y_p) \left(\frac{2.7255K}{T_\gamma^0}\right)^3. \tag{11}$$

The CMB also encodes the values of Y_p and $N_{\rm eff}$ at recombination. The effect of helium and thus Y_p is to set the number of plasma electrons per baryon. This controls the Thomson scattering mean free path $(\sigma_{\rm T} n_e)^{-1}$ that sets the scale at which the acoustic peaks are damped (exponentially) by photon diffusion. The effect of radiation and thus of $N_{\rm eff}$ is predominantly to increase the cosmic expansion rate via $H^2 \propto \rho$. This also affects the scale of damping onset, when the diffusion length is comparable to the sound horizon (Hou *et al.*, 2013). Thus, measurements of the CMB damping tail at small angular scales (high ℓ) probe both Y_p and $N_{\rm eff}$. In fact, the CMB determinations of these quantities are strongly anticorrelated—a higher Y_p implies a lower diffusion mean free path, which is equivalent to a larger sound horizon $\sim \int da/aH$ and thus lower $N_{\rm eff}$.

Since the first WMAP results in 2003 (Spergel *et al.*, 2003) sharply measured the first acoustic peaks, the CMB has determined η more precisely than BBN. Moreover, both ground-based and *Planck* data now measure the damping tail with sufficient accuracy to simultaneously probe all of $(\Omega_{\rm b}h^2, Y_p, N_{\rm eff})$ (Keisler *et al.*, 2011; Sievers *et al.*, 2013; Ade *et al.*, 2015). Of course, BBN demands an essentially unique relationship among these quantities. Thus, it is now possible to meaningfully test BBN and thus cosmology via CMB measurements alone.

We adopt CMB determinations of $(\Omega_{\rm b}h^2, Y_p, N_{\rm eff})$ from *Planck* 2015 data, as described in detail in Sec. IV.C. We note in passing that these CMB constraints rely on the present CMB temperature T_γ^0, which is held fixed in the *Planck* analysis we use. In the future, T_γ^0 should be varied in the CMB data evaluation in order to provide the most stringent constraint on the relative number of baryons in the Universe.

IV. THE LIKELIHOOD ANALYSIS

As data analysis improved, theoretical studies of BBN moved toward a more rigorous approach using Monte Carlo techniques in likelihood analyses (Krauss and Romanelli, 1990; Smith, Kawano, and Malaney, 1993; Kernan and Krauss, 1994; Krauss and Kernan, 1995; Fields and Olive, 1996; Fields *et al.*, 1996; Hata *et al.*, 1996). Thus, in order to make quantitative statements about the light-element predictions and convolutions with CMB constraints, we need probability distributions for our BBN predictions, for the light-element observations, and CMB-constrained parameters. We discuss here how we propagate nuclear reaction rate uncertainties into the BBN light-element abundance predictions, how we determine the CMB-parameter likelihood distributions, and how we combine them to make stronger constraints.

A. Monte Carlo predictions for the light elements

The dominant source of uncertainty in the BBN light-element predictions stems from experimental uncertainties of nuclear reaction rates. We propagate these uncertainties by randomly drawing rates according to their adopted probability distributions for each BBN evaluation. We choose a Monte Carlo analysis with $N = 10\,000$ runs, keeping the error in the mean and error in the error at the 1% level. It is important that we use the same random numbers for each set of parameters (η, N_ν). This helps remove any extra noise from the Monte Carlo predictions and allows for smooth interpolations between parameter points.

For each grid point of parameter values we calculate the means and covariances of the light-element abundance predictions. We add the $1/\sqrt{N}$ errors in quadrature to our evaluated uncertainties on the light-element predictions. We have examined the light-element abundance distributions, by calculating higher-order statistics (skewness and kurtosis), and by histogramming the resultant Monte Carlo points and verified that they are well approximated with log-normal or Gaussian distributions.

In standard BBN, the baryon-to-photon ratio (η) is the only free parameter of the theory. Our Monte Carlo error propagation is summarized in Fig. 1, which plots the light-element abundances as a function of the baryon density (upper scale) and η (lower scale). The abundance for He is shown as the mass fraction Y_p, while the abundances of the remaining isotopes of D, ^{3}He, and ^{7}Li are shown as abundances by a number relative to H. The thickness of the curves shows the

$\pm 1\sigma$ spread in the predicted abundances. These results assume $N_\nu = 3$ and the current measurement of the neutron lifetime $\tau_n = 880.3 \pm 1.1$ s.

Using a Monte Carlo approach also allows us to extract sensitivities of the light-element predictions to reaction rates and other parameters. The sensitivities are defined as the logarithmic derivatives of the light-element abundances with respect to each variation about our fiducial model parameters (Fiorentini *et al.*, 1998), yielding a simple relation for extrapolating about the fiducial model:

$$X_i = X_{i,0} \prod_n \left(\frac{p_n}{p_{n,0}} \right)^{\alpha_n}, \tag{12}$$

where X_i represents either the helium mass fraction or the abundances of the other light elements by number. The p_n represent input quantities to the BBN calculations (η, N_ν, τ_n) and the gravitational constant[5] G_N as well as key nuclear rates which affect the abundance X_i. $p_{n,0}$ refers to our standard input value. The information contained in Eqs. (13)–(17) is summarized in Table III:

$$Y_p = 0.24703 \left(\frac{10^{10}\eta}{6.10} \right)^{0.039} \left(\frac{N_\nu}{3.0} \right)^{0.163} \left(\frac{G_N}{G_{N,0}} \right)^{0.35} \left(\frac{\tau_n}{880.3s} \right)^{0.73} [p(n,\gamma)d]^{0.005} [d(d,n)^3\mathrm{He}]^{0.006} [d(d,p)t]^{0.005}, \tag{13}$$

$$\frac{\mathrm{D}}{\mathrm{H}} = 2.579 \times 10^{-5} \left(\frac{10^{10}\eta}{6.10} \right)^{-1.60} \left(\frac{N_\nu}{3.0} \right)^{0.395} \left(\frac{G_N}{G_{N,0}} \right)^{0.95} \left(\frac{\tau_n}{880.3s} \right)^{0.41} [p(n,\gamma)d]^{-0.19} [d(d,n)^3\mathrm{He}]^{-0.53} [d(d,p)t]^{-0.47} \times [d(p,\gamma)^3\mathrm{He}]^{-0.31} [^3\mathrm{He}(n,p)t]^{0.023} [^3\mathrm{He}(d,p)^4\mathrm{He}]^{-0.012}, \tag{14}$$

$$\frac{^3\mathrm{He}}{\mathrm{H}} = 9.996 \times 10^{-6} \left(\frac{10^{10}\eta}{6.10} \right)^{-0.59} \left(\frac{N_\nu}{3.0} \right)^{0.14} \left(\frac{G_N}{G_{N,0}} \right)^{0.34} \left(\frac{\tau_n}{880.3s} \right)^{0.15} [p(n,\gamma)d]^{0.088} [d(d,n)^3\mathrm{He}]^{0.21} [d(d,p)t]^{-0.27} \times [d(p,\gamma)^3\mathrm{He}]^{0.38} [^3\mathrm{He}(n,p)t]^{-0.17} [^3\mathrm{He}(d,p)^4\mathrm{He}]^{-0.76} [t(d,n)^4\mathrm{He}]^{-0.009}, \tag{15}$$

$$\frac{^7\mathrm{Li}}{\mathrm{H}} = 4.648 \times 10^{-10} \left(\frac{10^{10}\eta}{6.10} \right)^{2.11} \left(\frac{N_\nu}{3.0} \right)^{-0.284} \left(\frac{G_N}{G_{N,0}} \right)^{-0.73} \left(\frac{\tau_n}{880.3s} \right)^{0.43} [p(n,\gamma)d]^{1.34} [d(d,n)^3\mathrm{He}]^{0.70} [d(d,p)t]^{0.065} \times [d(p,\gamma)^3\mathrm{He}]^{0.59} [^3\mathrm{He}(n,p)t]^{-0.27} [^3\mathrm{He}(d,p)^4\mathrm{He}]^{-0.75} [t(d,n)^4\mathrm{He}]^{-0.023} \times [^3\mathrm{He}(\alpha,\gamma)^7\mathrm{Be}]^{0.96} [^7\mathrm{Be}(n,p)^7\mathrm{Li}]^{-0.71} [^7\mathrm{Li}(p,\alpha)^4\mathrm{He}]^{-0.056} [t(\alpha,\gamma)^7\mathrm{Li}]^{0.030}, \tag{16}$$

$$\frac{^6\mathrm{Li}}{\mathrm{H}} = 1.288 \times 10^{-13} \left(\frac{10^{10}\eta}{6.10} \right)^{-1.51} \left(\frac{N_\nu}{3.0} \right)^{0.60} \left(\frac{G_N}{G_{N,0}} \right)^{1.40} \left(\frac{\tau_n}{880.3s} \right)^{1.37} [p(n,\gamma)d]^{-0.19} [d(d,n)^3\mathrm{He}]^{-0.52} [d(d,p)t]^{-0.46} \times [d(p,\gamma)^3\mathrm{He}]^{-0.31} [^3\mathrm{He}(n,p)t]^{0.023} [^3\mathrm{He}(d,p)^4\mathrm{He}]^{-0.012} [d(\alpha,\gamma)^6\mathrm{Li}]^{1.00}. \tag{17}$$

B. The neutron mean lifetime

As noted in the Introduction, the value of the neutron mean lifetime has had a turbulent history. Unfortunately, the predictions of SBBN remain sensitive to this quantity. This sensitivity is displayed in the scatter plot of our Monte Carlo error propagation with fixed $\eta = 6.10 \times 10^{-10}$ in Fig. 2. The correlation between the neutron mean lifetime and ^{4}He abundance prediction is clear. The correlation is not infinitesimally narrow because other reaction rate uncertainties significantly contribute to the total uncertainty in ^{4}He.

C. *Planck* likelihood functions

For this paper, we consider two sets of *Planck* Markov chain data, one for standard BBN (SBBN) and one for

TABLE III. The sensitivities α_n's defined in Eq. (12) for each of the light-element abundance predictions, varied with respect to key parameters and reaction rates.

Variant	Y_p	D/H	^{3}He/H	^{7}Li/H	^{6}Li/H
η (6.1×10^{-10})	0.039	−1.598	−0.585	2.113	−1.512
N_ν (3.0)	0.163	0.395	0.140	−0.284	0.603
G_N	0.354	0.948	0.335	−0.727	1.400
n decay	0.729	0.409	0.145	0.429	1.372
$p(n,\gamma)d$	0.005	−0.194	0.088	1.339	−0.189
$^3\mathrm{He}(n,p)t$	0.000	0.023	−0.170	−0.267	0.023
$^7\mathrm{Be}(n,p)^7\mathrm{Li}$	0.000	0.000	0.000	−0.705	0.000
$d(p,\gamma)^3\mathrm{He}$	0.000	−0.312	0.375	0.589	−0.311
$d(d,\gamma)^4\mathrm{He}$	0.000	0.000	0.000	0.000	0.000
$^7\mathrm{Li}(p,\alpha)^4\mathrm{He}$	0.000	0.000	0.000	−0.056	0.000
$d(\alpha,\gamma)^6\mathrm{Li}$	0.000	0.000	0.000	0.000	1.000
$t(\alpha,\gamma)^7\mathrm{Li}$	0.000	0.000	0.000	0.030	0.000
$^3\mathrm{He}(\alpha,\gamma)^7\mathrm{Be}$	0.000	0.000	0.000	0.963	0.000
$d(d,n)^3\mathrm{He}$	0.006	−0.529	0.213	0.698	−0.522
$d(d,p)t$	0.005	−0.470	−0.265	0.065	−0.462
$t(d,n)^4\mathrm{He}$	0.000	0.000	−0.009	−0.023	0.000
$^3\mathrm{He}(d,p)^4\mathrm{He}$	0.000	−0.012	−0.762	−0.752	−0.012

[5]In models beyond the standard model, one may also consider variations of the gravitational constant (for fixed nucleon masses). See Yang *et al.* (1979), Accetta, Krauss, and Romanelli (1990), Sarkar (1996), Copi, Davis, and Krauss (2004), and Cyburt *et al.* (2005) for BBN limits on variations of G_N.

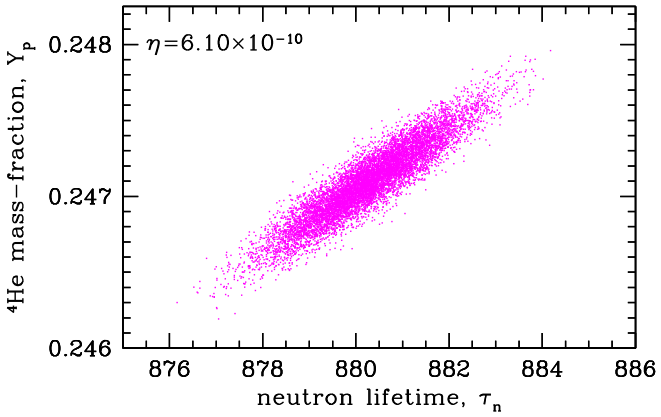

FIG. 2. The sensitivity of the ^{4}He abundance to the neutron mean lifetime, as shown through a scatter plot of our Monte Carlo error propagation.

nonstandard BBN (NBBN), where we allow the number of neutrino flavors to differ from 3. There are many possible choices that could be made for using Planck data sets. In particular, Planck offers results based on several combinations of their data such as including polarization, lensing, baryon acoustic oscillations, etc. Here we choose the CMB data set that uses both temperature and polarization (E-mode) data, corresponding to the *Planck* $TT, TE, EE + \mathrm{low}P$ set. This is labeled as `plikHM_TTTEEE_lowTEB` in the Planck archive. Using the *Planck* Markov chain data (Planck Collaboration, 2015), we constructed the multidimensional likelihoods for the following extended parameter chains, **base_yhe** and **base_nnu_yhe**, for the `plikHM_TTTEEE_lowTEB` data set. As noted earlier, we do not use the *Planck* base chain, as it assumes a BBN relationship between the helium abundance and the baryon density. **base_yhe** refers to the data chain that allows the helium abundance to vary independently while fixing $N_{\rm eff} = 3.046$, and **base_nnu_yhe** allows both the helium abundance and the number of effective degrees of freedom to vary independently.

From these two parameter sets we have the following two- and three-dimensional likelihoods from the CMB: $\mathcal{L}_{\rm PLA-base\_yhe}(\omega_b, Y_p)$ and $\mathcal{L}_{\rm PLA-base\_nnu\_yhe}(\omega_b, Y_p, N_\nu)$. The two-dimensional **base_yhe** likelihood $\mathcal{L}_{\rm PLA-base\_yhe}(\omega_b, Y_p)$ is well represented by a 2D correlated Gaussian distribution, with means and standard deviations for the baryon density and ^{4}He mass fraction

$$\omega_b = 0.022\,305 \pm 0.000\,225, \tag{18}$$

$$Y_p = 0.250\,03 \pm 0.013\,67, \tag{19}$$

and a correlation coefficient $r \equiv \mathrm{cov}(\omega_b, Y_p)/\sqrt{\mathrm{var}(\omega_b)\mathrm{var}(Y_p)} = +0.7200$. Recall that $\omega_b = \Omega_B h^2$. These likelihoods are plotted in Figs. 4 and 6.

The two parameter data can be marginalized to yield one-dimensional likelihood functions for η. The peak and 1σ spread in η are given in the first row of Table IV. The following rows correspond to different determinations of η. In the second to fourth rows, no CMB data are used. That is, we fix η only from the observed abundances of ^{4}He, D, or both. Notice, for example, in row 2, the value for η is low and has a large uncertainty. This is due to the slightly low value for the observational abundance (7) and the logarithmic dependence of Y_p on η. We see again that BBN+Y_p is a poor baryometer. This is described in more detail in Sec. IV.D. Row 5 uses the BBN relation between η and Y_p, but no observational input from Y_p is used. This is closest to the *Planck* determination found in Table 4 and Eq. (72) of Ade *et al.* (2015), although here Y_p was taken to be free and the value of η in the table is a result of marginalization over Y_p. This accounts for the very small difference in the results for η: $\eta_{10} = 6.09$ (*Planck*) and $\eta_{10} = 6.10$ (Table IV). Rows 6–8 add the observational determinations of ^{4}He, D, and the combination. As one can see, the inclusion of the observational data does very little to affect the determination of η and thus we use $\eta_{10} = 6.10$ as our fiducial baryon-to-photon ratio.

TABLE IV. Constraints on the baryon-to-photon ratio, using different combinations of observational constraints. We have marginalized over Y_p to create 1D η likelihood distributions.

Constraints used	$\eta \times 10^{10}$	$\Omega_B h^2$
CMB only	6.108 ± 0.060	$0.022\,31 \pm 0.000\,22$
BBN + Y_p	$4.87^{+2.46}_{-1.54}$	$0.0178^{+0.0090}_{-0.0056}$
BBN + D	6.180 ± 0.195	$0.022\,57 \pm 0.000\,71$
BBN + Y_p + D	6.172 ± 0.195	$0.022\,54 \pm 0.000\,71$
CMB + BBN	6.098 ± 0.042	$0.022\,27 \pm 0.000\,15$
CMB + BBN + Y_p	6.098 ± 0.042	$0.022\,27 \pm 0.000\,15$
CMB + BBN + D	6.102 ± 0.041	$0.022\,29 \pm 0.000\,15$
CMB + BBN + Y_p + D	6.101 ± 0.041	$0.022\,28 \pm 0.000\,15$

The three-dimensional **base_nnu_yhe** likelihood $\mathcal{L}_{\rm PLA-base\_nnu\_yhe}(\omega_b, Y_p, N_\nu)$ is close to, but not fully captured by, a simple 3D correlated Gaussian distribution. But since these distributions are single peaked and close to Gaussian, we can correct for the non-Gaussianity via a 3D Hermite expansion about a 3D correlated Gaussian base distribution. Details of this prescription are given in the Appendix.

The calculated mean values and standard deviations for these distributions are as follows:

$$\omega_b = 0.022\,212 \pm 0.000\,242, \tag{20}$$

$$N_{\rm eff} = 2.7542 \pm 0.3064, \tag{21}$$

$$Y_p = 0.261\,16 \pm 0.018\,12. \tag{22}$$

These values correspond to the peak of the likelihood distribution using CMB data alone. That is, no use is made of the correlation between the baryon density and the helium abundance through BBN. For this reason, the helium mass fraction is found to be rather high. Our value of $Y_p = 0.261 \pm 0.036(2\sigma)$ can be compared with the value given by the *Planck* Collaboration in Eq. (79) of Ade *et al.* (2015) with $Y_p = 0.263^{+0.034}_{-0.037}$.

In this case, we marginalize to form a 2D likelihood function to determine both η and $N_{\rm eff}$. As in the 1D case discussed previously, we can determine η and N_ν using CMB data alone. This result is shown in row 1 of Table V and does not use any correlation between η and Y_p. Note that the value

TABLE V. The marginalized most-likely values and central 68.3% confidence limits on the baryon-to-photon ratio and number of neutrinos, using different combinations of observational constraints.

Constraints used	η_{10}	$\Omega_B h^2$	N_ν
CMB only	6.08±0.07	0.02220±0.00026	$2.67^{+0.30}_{-0.27}$
BBN+Y_p+D	6.10±0.23	0.02228±0.00084	2.85±0.28
CMB+BBN	6.08±0.07	0.02220±0.00026	2.91±0.20
CMB+BBN+Y_p	6.07±0.06	0.02217±0.00022	2.89±0.16
CMB+BBN+D	6.07±0.07	0.02217±0.00026	2.90±0.19
CMB+BBN+Y_p+D	6.07±0.06	0.02217±0.00022	2.88±0.16

of N_ν given here differs from that in Eq. (21) since the value in the table comes from a marginalized likelihood function, where as the value in the equation does not. Row 2 uses only BBN and the observed abundances of ^{4}He and D with no direct information from the CMB. Rows 3–6 use the combination of the CMB data, together with the BBN relation between η and Y_p with and without the observational abundances as denoted. As one can see, opening up the parameter space to allow N_ν to float induces a relatively small drop η (by a fraction of 1σ) and the peak for N_ν is below the standard model value of 3 although consistent with that value within 1σ. These can be compared with Eqs. (75) and (76) in Ade *et al.* (2015).

Note that we have been careful to use the appropriate relation between η and ω_b via Eq. (11). Also, in our NBBN calculations we formally use the number of neutrinos, not the effective number of neutrinos, thus demanding the relation $N_{\rm eff} = 1.015\,333 N_\nu$. For the 2D **base_yhe** CMB likelihoods, we include the higher-order skewness and kurtosis terms to more accurately reproduce the tails of the distributions.

D. Results: The likelihood functions

Applying the formalism described previously, we derive the likelihood functions for SBBN and NBBN that are our central results. Depending on which quantity we marginalize over, we can form a likelihood function of η by integrating over abundances as we do later, or by integrating over the baryon density to obtain a likelihood function for each element species. Turning first to SBBN, we fix $N_\nu = 3$ and use the *Planck* determination of η as the sole input to BBN in order to derive CMB + BBN predictions for each light element. That is, for each light-element species X_i we evaluate the likelihood

$$\mathcal{L}(X_i) \propto \int \mathcal{L}_{\rm PLA-base\_yhe}(\omega_b, Y_p)\mathcal{L}_{\rm BBN}(\eta; X_i)d\eta, \qquad (23)$$

where $\mathcal{L}_{\rm BBN}(\eta; X_i)$ comes from our BBN Monte Carlo prediction, and where we use the $\eta - \omega_{\rm b}$ relation in Eq. (11). In the case of ^{4}He, we use only the CMB η to determine the $X_i = Y_{p,\rm BBN}$ prediction and compare this to the CMB-only prediction.

The resulting CMB + BBN abundance likelihoods appear as the dark-shaded (solid line) curves in Fig. 3, which also shows the observational abundance constraints (Sec. III) in the light-shaded (yellow, dashed-line) curves. In Fig. 3(a), we see

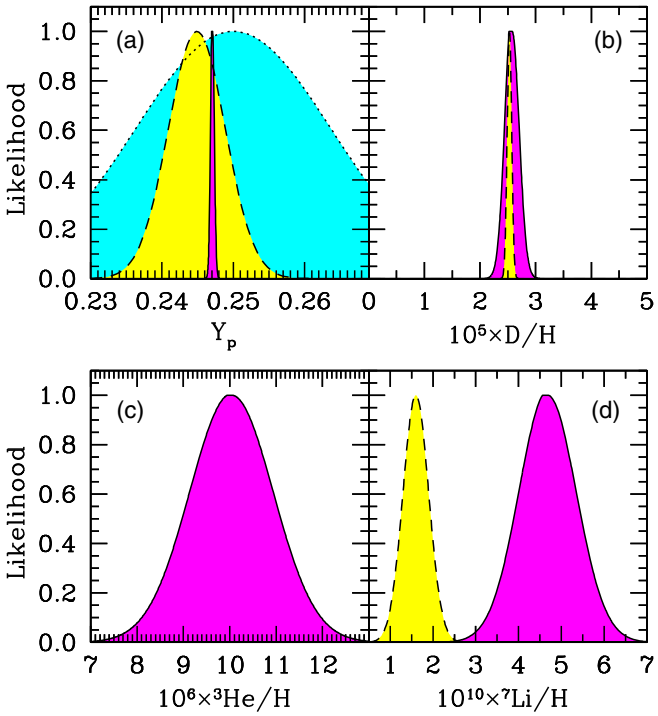

FIG. 3. Light-element predictions using the CMB determination of the cosmic baryon density. Shown are likelihoods for each of the light nuclides, normalized to show a maximum value of 1. The solid-lined, dark-shaded (purple) curves are the BBN + CMB predictions, based on *Planck* inputs as discussed in the text. The dashed-lined, light-shaded (yellow) curves show astronomical measurements of the primordial abundances, for all but ^{3}He where reliable primordial abundance measures do not exist. For ^{4}He, the dotted-lined, medium-shaded (cyan) curve shows the CMB determination of ^{4}He.

that the ^{4}He BBN + CMB likelihood is markedly more narrow than its observational counterpart, but the two are in near-perfect agreement. The medium-shaded (cyan, dotted line) curve in this panel is the CMB-only Y_p prediction, which is the least precise but also completely consistent with the other distributions. Figure 3(b) displays the dramatic consistency between the CMB + BBN deuterium prediction and the observed high-z abundance. Moreover, we see that the D/H observations are substantially more precise than the theory. Figure 3(c) shows the primordial ^{3}He prediction, for which there is no reliable observational test at present. Finally, Fig. 3(d) reveals a sharp discord between the BBN + CMB prediction for ^{7}Li and the observed primordial abundance—the two likelihoods are essentially disjoint.

Figure 3 represents not only a quantitative assessment of the concordance of BBN, but also a test of the standard big bang cosmology. If we limit our attention to each element in turn, we are struck by the spectacular agreement between D/H observations at $z \sim 3$ and the BBN + CMB predictions combining physics at $z \sim 10^{10}$ and $z \sim 1000$. The consistency among all three Y_p determinations is similarly remarkable, and the joint concordance between D and ^{4}He represents a nontrivial success of the hot big bang model. Yet this concordance is not complete: the pronounced discrepancy

in ^{7}Li measures represents the lithium problem discussed later (Sec. V). This casts a shadow of doubt over SBBN itself, pending a firm resolution of the lithium problem, and until then the BBN/CMB concordance remains an incomplete success for cosmology.

Quantitatively, the likelihoods in Fig. 3 are summarized by the predicted abundances

$$Y_p = 0.247\,09 \pm 0.000\,25, \tag{24}$$

$$\mathrm{D/H} = (2.58 \pm 0.13) \times 10^{-5}, \tag{25}$$

$$^3\mathrm{He/H} = (10.039 \pm 0.090) \times 10^{-6}, \tag{26}$$

$$^7\mathrm{Li/H} = (4.68 \pm 0.67) \times 10^{-10}, \tag{27}$$

$$\log_{10}(^6\mathrm{Li/H}) = -13.89 \pm 0.20, \tag{28}$$

where the central values give the mean, and the errors the 1σ variance. The slight differences from the values in Table II arise due to the Monte Carlo averaging procedure here as opposed to evaluating the abundance using central values of all inputs at a single η.

We see that the BBN/CMB comparison is enriched now that the CMB has achieved an interesting sensitivity to Y_p as well as η. This interplay is further illustrated in Fig. 4, which shows 2D likelihood contours in the (η, Y_p) plane, still for fixed $N_\nu = 3$. The *Planck* contours show a positive correlation between the CMB-determined baryon density and the helium abundance. Also plotted is the BBN relation for $Y_p(\eta)$, which

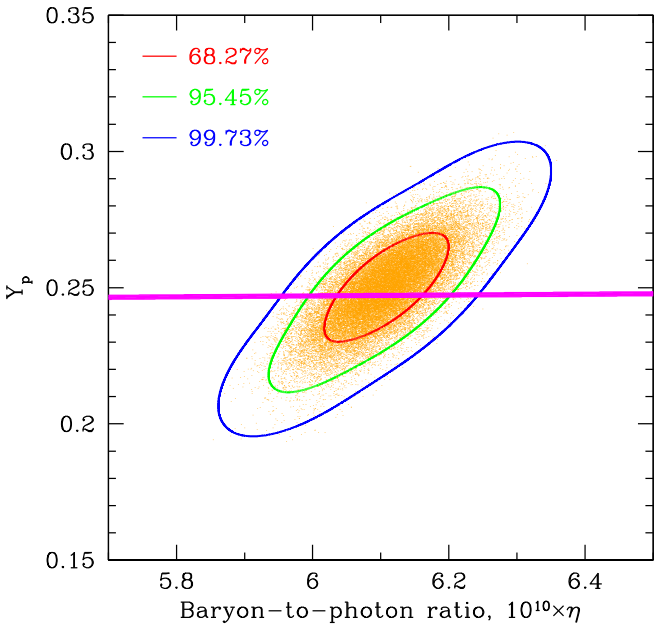

FIG. 4. The 2D likelihood function contours derived from the *Planck* Markov chain Monte Carlo **base_yhe** with fixed $N_\nu = 3$ (points). The correlation between Y_p and η is evident. The 3σ BBN prediction for the helium mass fraction is shown with the colored band. We see that including the BBN $Y_p(\eta)$ relation significantly reduces the uncertainty in η due to the CMB $Y_p - \eta$ correlation.

for SBBN is a *zero-parameter curve* that is very tight even including its small width due to nuclear reaction rate uncertainties. We see that the curve goes through the heart of the CMB predictions, which represents a novel and nontrivial test of SBBN based entirely on CMB data without any astrophysical input. This agreement stands as a triumph for SBBN and the hot big bang and illustrates the still-growing power of the CMB as a cosmological probe.

Thus far we have used the CMB η as an input to BBN; we conclude this section by studying the constraints on η when jointly using BBN theory, light-element abundances, and the CMB in various combinations. Figure 5 shows the η likelihoods that result from a set of such combinations. Setting aside at first the CMB, the BBN + X curves show the combination of BBN theory and astrophysical abundance observations, $\mathcal{L}_{\mathrm{BBN}+X}(\eta) = \int \mathcal{L}_{\mathrm{BBN}}(\eta, X)\mathcal{L}_{\mathrm{obs}}(X)dX$, with $X \in (Y_p, \mathrm{D/H})$. The CMB-only curve marginalizes over the *Planck* Y_p values $\mathcal{L}_{\mathrm{CMB-only}}(\eta) = \int \mathcal{L}_{\mathrm{PLA-base\_yhe}}(\omega_b, Y_p)dY_p$ where we use the $\eta - \omega_\mathrm{b}$ relation in Eq. (11). The BBN + CMB curve adds the BBN $Y_p(\eta)$ relation. Finally, BBN + CMB + D also includes the observed primordial deuterium.

We see in Fig. 5 that of the primordial abundance observations, deuterium is the only useful "baryometer," due to its strong dependence on η in the Schramm plot (Fig. 1). By contrast, ^{4}He alone offers no useful constraint on η, tracing back to the weak $Y_p(\eta)$ trend in Fig. 1. The CMB alone has now surpassed BBN + D in measuring the cosmic baryon content, but an even stronger limit comes from BBN + CMB. As seen in Fig. 4, this tightens the η constraint due to the CMB correlation between Y_p and η. Finally BBN + CMB + D provides only negligibly stronger limits. The peaks of the likelihoods correspond to the values in Table IV, and the tightest constraints are all consistent with our adopted central value $\eta = 6.10 \times 10^{-10}$. In comparison with Fig. 1 of Di Valentino *et al.* (2014), the BBN-only lower limit is somewhat weaker, but we obtain a similar result when the CMB is included.

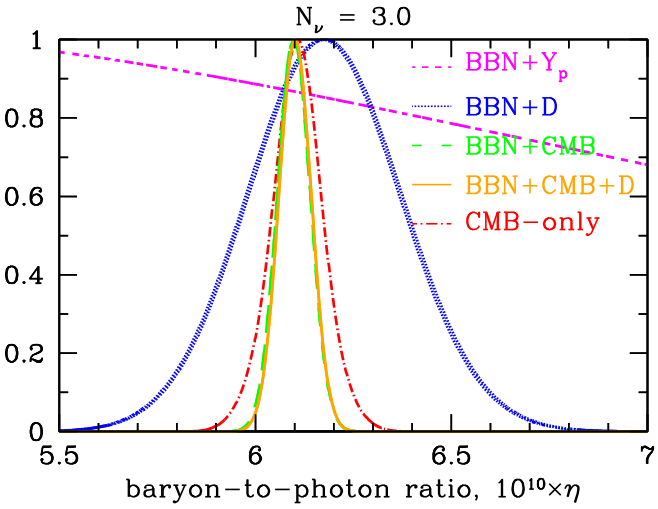

FIG. 5. The likelihood distributions of the baryon-to-photon ratio parameter η given various CMB and light-element abundance constraints.

V. THE LITHIUM PROBLEM

As seen in Fig. 3, the observed primordial lithium abundance differs sharply from the BBN + CMB prediction (Cyburt, Fields, and Olive, 2008). This discrepancy constitutes the lithium problem, which was foreshadowed before CMB determinations of η and has persisted over the dozen years since the first WMAP data release. For a detailed recent review of the lithium problem, see Fields (2011). Here we briefly summarize the current status.

The most conventional means to resolve the primordial lithium problem invokes large lithium depletion in halo stars (Pinsonneault *et al.*, 1999, 2002; Vauclair and Charbonnel, 1998; Richard, Michaud, and Richer, 2005; Korn *et al.*, 2006; García Peréz *et al.*, 2008). As noted previously (Sec. III.C), recent observations of the Spite plateau meltdown at very low metallicity $[\mathrm{Fe/H}] < -3$ seem to demand that some stars have depleted their lithium (Aoki *et al.*, 2009; Sbordone *et al.*, 2010; Frebel and Norris, 2015). Could the other plateau halo stars have also destroyed their lithium? Such a scenario cannot be ruled out, but raises other questions that remain unanswered: why is the Li/H dispersion so small at metallicities above the meltdown? And why is there a "lithium desert" with almost no stars having lithium abundances between the plateau and the primordial abundance?

It is worthwhile to find other sites for Li/H measurements, as clearly halo star lithium depletion is theoretically complex and observationally challenging. Unfortunately, the CMB itself does not yet provide an observable signature of primordial lithium (Switzer and Hirata, 2005). However, a promising new direction is the observation of interstellar lithium in low-metallicity or high-z galaxies (Friedel, Kemball, and Fields, 2011). Interstellar measurements in the small Magellanic Cloud (SMC) (metallicity $\sim 1/4$ solar) find $\mathrm{Li/H}_{\mathrm{ISM,SMC}} = (4.8 \pm 1.8) \times 10^{-10}$ (Howk *et al.*, 2012). This value is consistent with the CMB + BBN primordial abundance, but the SMC is far from primordial, with a metallicity of about $1/4$ solar. Indeed, the SMC interstellar lithium abundance agrees with that of Milky Way stars at the same [Fe/H], which are disk (population I) stars in which Li/H is rising from the Spite plateau due to Galactic production. Thus we see consistency between lithium abundances at the same metallicity, but measured in very different systems with very different systematics. This strongly suggests that stellar lithium depletion has not been underestimated, at least not down to this metallicity. Moreover, this observation serves as a proof-of-concept demonstration that measurements of interstellar lithium in galaxies with lower metallicities could strongly test stellar depletion and potentially rule out this solution to the lithium problem.

Another means of resolving the lithium problem within the context of the standard cosmology and standard model microphysics is to alter the BBN theory predictions due to revisions in nuclear reaction rates (Cyburt, Fields, and Olive, 2004; Boyd *et al.*, 2010; Coc *et al.*, 2012). But as seen, all of the reactions that are ordinarily the most important for BBN have been well measured at the energies of interest. Typically, cross sections are known to $\sim 10\%$ or better, and these errors are already folded into Fig. 3. A remaining possibility is that a reaction thought to be unimportant could contain a *resonance* heretofore unknown, which could boost its cross section enormously, analogously to the celebrated Hoyle ^{12}C resonance that dominates the $3\alpha \to {}^{12}\mathrm{C}$ rate (Hoyle, 1954).

In BBN, the densities and time scales prior to nuclear freezeout are such that only two-body reactions are important, and it is possible to systematically study all two-body reactions that enhance the destruction of ^{7}Be. A small number of candidates emerge, for which one can make definite predictions of the needed resonant state energy and width. These involve three compound states: $^7\mathrm{Be} + d \to {}^9\mathrm{B}^*$, $^7\mathrm{Be} + t \to {}^{10}\mathrm{B}^*$, and $^7\mathrm{Be} + {}^3\mathrm{He} \to {}^{10}\mathrm{C}^*$, with various possible exit channels (Chakraborty, Fields, and Olive, 2011; Broggini *et al.*, 2012; Cyburt and Pospelov, 2012). However, measurements in $^7\mathrm{Be}(d,d)^7\mathrm{Be}$ (O'Malley *et al.*, 2011), $^9\mathrm{Be}(^3\mathrm{He},t)^9\mathrm{B}$ (Kirsebom and Davids, 2011), and an R-matrix analysis of ^{9}B (Paris *et al.*, 2013) all rule out a ^{9}B resonance. Similarly, ^{10}C data rule out the needed resonance in ^{10}C (Hammache *et al.*, 2013). The upshot is that a "nuclear option" to the lithium problem is essentially excluded.

It is thus a real possibility that the lithium problem may point to new physics at play during or after nucleosynthesis. A number of possible solutions have been proposed and are discussed in the reviews cited previously. Here we simply note that a challenge to all such models is that they must reduce ^{7}Li substantially, yet not perturb the other light elements unacceptably. Generally, there is a tradeoff between ^{7}Be destruction and D production (Ellis, Olive, and Vangioni, 2005; Olive *et al.*, 2012; Coc *et al.*, 2014; Kusakabe, Cheoun, and Kim, 2014). This arises because ^{4}He disruption creates both D and neutrons as fragments. These neutrons, as well as nonthermal neutrons produced in the case of hadronic decays, then lead to mass-7 destruction via $^7\mathrm{Be}(n,p)^7\mathrm{Li}(p,\alpha)^4\mathrm{He}$. Essentially all successful models drive D/H to the maximum abundance allowed by observations. However, the new very precise D/H measurements (Sec. III.B) dramatically reduce the allowed perturbations and challenge most of the existing new-physics solutions to the lithium problem. It remains to be seen whether it is possible to introduce new physically motivated perturbations that satisfy the D/H constraint while still solving or at least substantially reducing the lithium problem.

VI. LIMITS ON N_{eff}

Before concluding, we consider a one-parameter extension of SBBN by allowing the number of relativistic degrees of freedom to differ from the standard model value of $N_\nu = 3$ and $N_{\mathrm{eff}} = 3.046$. Opening this degree of freedom has an impact on both the CMB and BBN. In Fig. 6, the thinner contours show the 2D likelihood distribution in the (η, N_ν) plane, using *Planck* data marginalizing over the CMB Y_p. We see that the CMB N_ν values are nearly uncorrelated with η. The thicker contours include BBN information and are discussed later.

Turning to the effects of N_ν on BBN, Eqs. (1)–(3) show that increasing the number of neutrino flavors leads to an increased Hubble parameter which in turn leads to an increased freeze-out temperature T_f. Since the neutron-to-proton ratio at freeze-out scales as $(n/p) \simeq e^{-\Delta m/T_f}$, higher T_f leads to higher (n/p) and thus higher Y_p (Shvartsman, 1969). As a

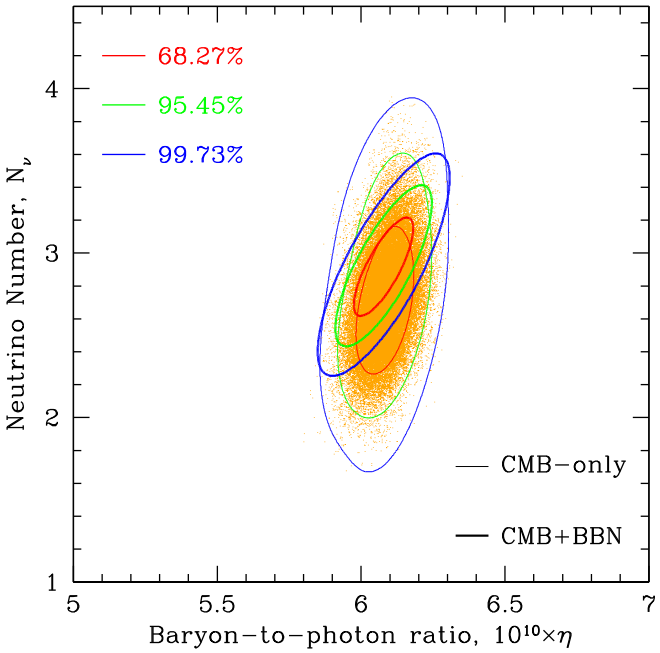

FIG. 6. The 2D likelihood function contours derived from the *Planck* Markov chain Monte Carlo **base_nnu_yhe**, marginalized over the CMB Y_p (points). Thin contours are for CMB data only, while thick contours use the BBN $Y_p(\eta)$ relation, assuming no observational constraints on the light elements. We see that whereas in the CMB-only case N_ν and η are almost uncorrelated, in the CMB + BBN case a stronger correlation emerges.

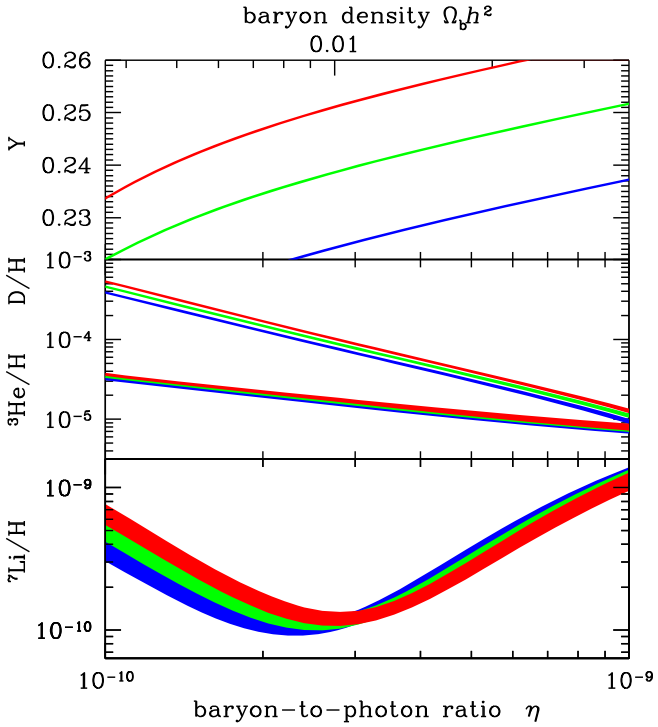

FIG. 7. The sensitivity of the light-element predictions to the number of neutrino species, similar to Fig. 1. Here abundances shown by different colored bands correspond to calculated abundances assuming $N_\nu = 2$, 3, and 4.

consequence, one can establish an upper bound to the number of neutrinos (Steigman, Schramm, and Gunn, 1977; Yang *et al.*, 1979) if in addition one has a lower bound on the baryon-to-photon ratio (Olive *et al.*, 1981) as the helium abundance also scales monotonically with η. The dependence of the helium mass fraction Y on both η and N_ν can be seen in Fig. 7, where we see the calculated value of Y for $N_\nu = 2$, 3, and 4 as depicted by the different colored curves. In the figure, one sees not only the monotonic growth of Y with η, but also the strong sensitivity of Y with N_ν. The importance of a lower bound on η (or better yet fixing η) is apparent in setting an upper bound on N_ν. Prior to CMB determinations of η, the lower bound on η could be set using a combination of D and ^{3}He observations enabling a limit of $N_\nu < 4$ (Yang *et al.*, 1984; Steigman *et al.*, 1986) given the estimated uncertainties in Y_p at the time. More aggressive estimates of an upper bound on the helium mass fraction led to tighter bounds on N_ν (Olive *et al.*, 1990; Walker *et al.*, 1991; Kernan and Krauss, 1994; Krauss and Kernan, 1995; Olive and Steigman, 1995). The bounds on N_ν became more rigorous when likelihood techniques were introduced (Kernan and Krauss, 1994; Krauss and Kernan, 1995; Sarkar, 1996; Copi, Schramm, and Turner, 1997; Olive and Thomas, 1997, 1999; Burles *et al.*, 1999; Lisi, Sarkar, and Villante, 1999; Cyburt, Fields, and Olive, 2002; Cyburt *et al.*, 2005; Mangano and Serpico, 2011).

While the dependence of Y_p on N_ν is well documented, we also see from Fig. 7 there is a non-negligible effect on D and ^{7}Li from changes in N_ν (Cyburt, Fields, and Olive, 2002). In particular, while the sensitivity of D to N_ν is not as great as that of Y_p, the deuterium abundance is measured much more accurately and as a result the constraint on N_ν is now due to both abundance determinations as can be discerned from Table V.

By marginalizing over the baryon density, we can form 1D likelihood functions for N_ν. These are shown in Fig. 8. In the left panel, we show the CMB-only result by the dashed blue curve. Recall that this uses no BBN correlation between the baryon density and helium abundance. While the peak of the likelihood for this case is the lowest of the cases considered ($N_\nu = 2.67$) its uncertainty (≈ 0.30) makes it consistent with the standard model. The position of the peak of the likelihood function is given in Table V for this case as well as the other cases considered in the figures. In contrast the dot-dashed red curve shows the limit we obtain purely from matching the BBN calculations with the observed abundances of helium and deuterium. In this case, the fact that the peak of the likelihood function is at $N_\nu = 2.85$ can be traced directly to the fact that the central helium abundance is $Y_p = 0.2449$. Given the sensitivity of Y_p to N_ν found in Eq. (13), the drop in N_ν from the standard model value of 3.0 compensates for a helium abundance below the standard model prediction closer to 0.247. Nevertheless, the uncertainty again places the standard model within 1σ of the distribution peak. The remaining cases displayed (solid green curve) correspond to combining the CMB data with BBN. There are four solid green curves in the left panel and these have been isolated in the right panel for better clarity. As one can see, once one combines the BBN relation between helium and the baryon

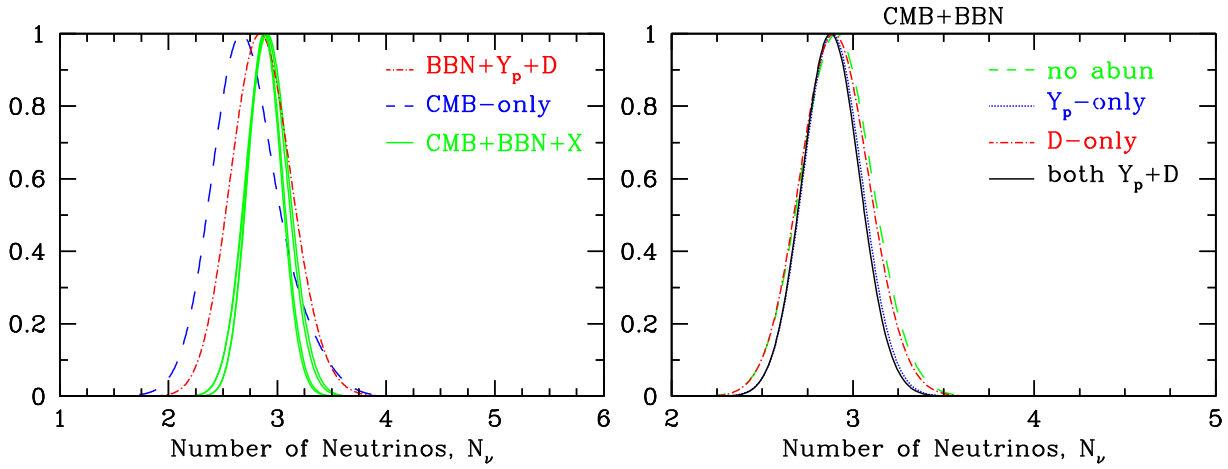

FIG. 8. The marginalized distributions for the number of neutrinos, given different combinations of observational constraints. The left panel shows the likelihood function in the case where only CMB data are used (dashed blue curve), only BBN and abundance data are used (dot-dashed red curve), and when a combination of BBN and CMB data is used (solid green curve). The four solid green curves are shown again in the right panel for better clarity.

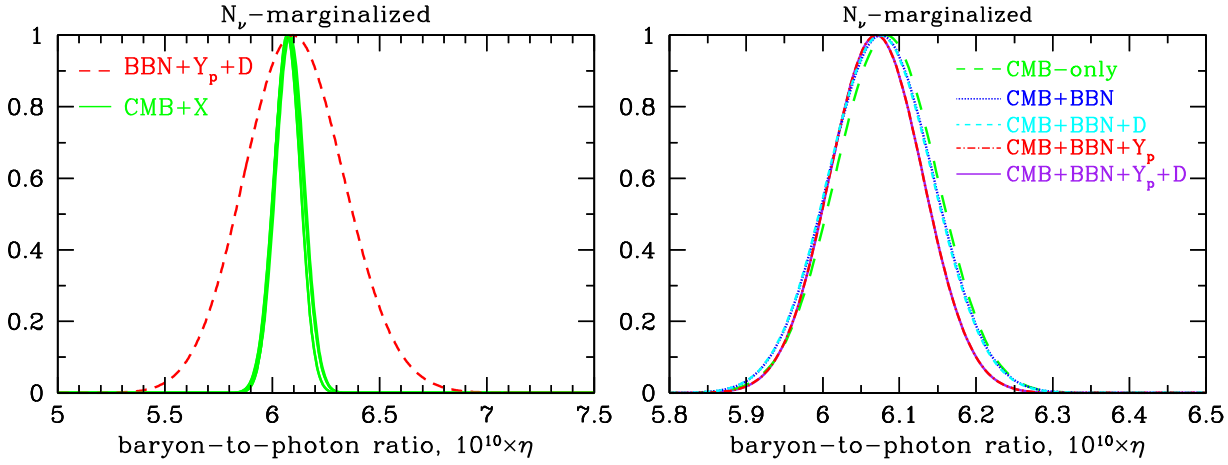

FIG. 9. The marginalized distributions for the baryon-to-photon ratio (η), given different combinations of observational constraints.

density, the actual abundance determinations have only a secondary effect in determining N_ν which takes values between 2.88 and 2.91. Using the CMB, BBN, and the abundances of both D and ^{4}He yields the tightest constraint on the number of neutrino flavors $N_\nu = 2.88 \pm 0.16$, again consistent with the standard model.[6] It is interesting to note that because of the drop in Y_p in the most recent analysis (Aver, Olive, and Skillman, 2015), the 95% C.L. upper limit on N_ν is 3.20.

It is also possible to marginalize over the number of neutrino flavors and produce a 1D likelihood function for η_{10} as shown in Fig. 9. In the left panel, the broad distribution shown by the dashed red curve corresponds to the BBN plus abundance data constraint using no information from the CMB. Here the baryon density is primarily determined by the D/H abundance. When the CMB is added, the uncertainty in η drops dramatically (from 0.23 to 0.06 or 0.07) independent of whether abundance data are used. The five solid green curves are almost indistinguishable and are shown in more detail in the right panel. Once again the peaks of the likelihood distributions are given in Table V. The values of η are slightly lower than the standard model results discussed previously. This is due to the additional freedom in the likelihood distribution afforded by the additional parameter N_ν.

For completeness, we also show 2D likelihood contours in the $\eta_{10} - N_\nu$ plane in Fig. 10. The three panels show the effects of the constraints imposed by the helium and deuterium abundances. In the first panel, only the helium abundance constraints are applied. The thinner open curves are based on BBN alone. They appear open as the helium abundance alone is a poor baryometer as has been noted several times already.

[6]Of all the cases considered, the one that can best be compared with the results presented by the *Planck* Collaboration (Ade *et al.*, 2015) is the case CMB + BBN + D. We find $N_{\rm eff} = 2.94 \pm 0.38(2\sigma)$ while they quote $N_{\rm eff} = 2.91 \pm 0.37$. While we obtain similar results to other cases, direct comparison is complicated not only by the slight difference in the $\eta - Y$ relation due to different BBN codes, but also by the adopted value for primordial ^{4}He.

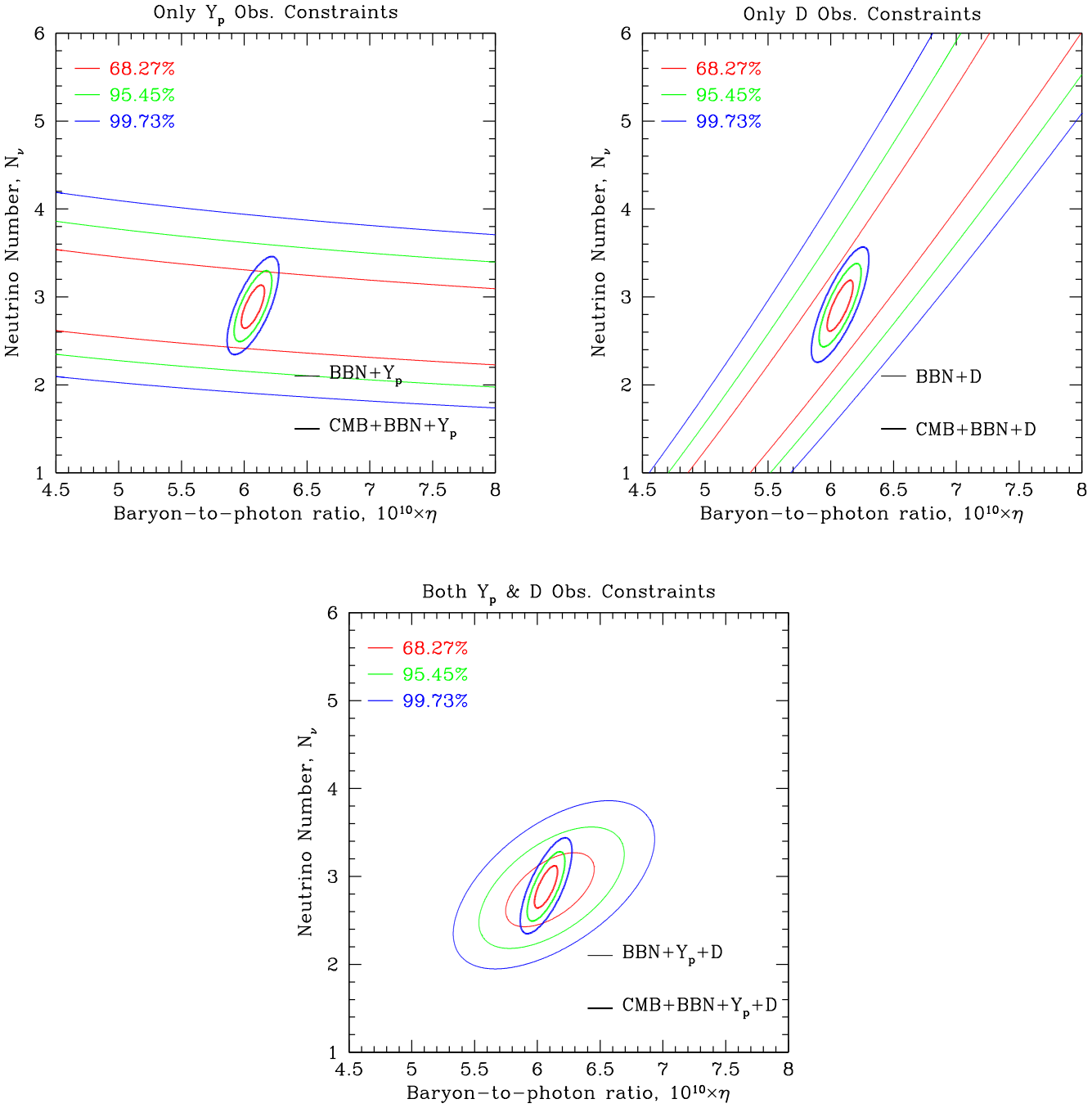

FIG. 10. The resulting two-dimensional likelihood functions for the baryon-to-photon ratio (η) and the number of neutrinos (N_ν), marginalized over the helium mass fraction Y_p, assuming different combinations of observational constraints on the light elements.

Without the CMB, the helium abundance data can produce an upper limit on N_ν of about 4 and depend weakly on the value of η. When the CMB data are applied, we obtain the thicker closed contours. The precision determination of η from the anisotropy spectrum correspondingly produces a very tight limit in N_ν. Here we see clearly that the standard model value of $N_\nu = 3$ falls well within the 68% C.L. contour.

The next panel of Fig. 10 shows the likelihood contours using the deuterium abundance data. Once again, the thin open curves are based on BBN alone. In this case, they appear open as the deuterium abundance is less sensitive to N_ν, although we note that the contours are not vertical and show some dependence on N_ν as discussed previously. In contrast to ^{4}He, for fixed N_ν, the deuterium abundance is capable of fixing η relatively precisely. Of course when the CMB data are added, the open contours collapse once again into a series of narrow ellipses.

The last panel of Fig. 10 shows the likelihood contours using both the ^{4}He and D/H data. In this case, even without any CMB input, we are able to obtain reasonably strong constraints on both η and N_ν as seen by the thin and larger ellipses. When the CMB data are added we recover the tight constraints which are qualitatively similar to those in the previous two panels.

Finally, in Fig. 6, we show the two-dimensional likelihood function using either CMB only (the thin outer curves which trace the density of models results of the Monte Carlo prediction) or the combination of CMB and BBN (tighter and thicker curves). In the latter case, no abundance data are used.

VII. DISCUSSION

Big bang cosmology can be said to have gone full circle. The prediction of the CMB was made in the context of the development of BBN and of what became big-bang cosmology (Alpher and Herman, 1948; Alpher, Bethe, and Gamow, 1948; Gamow, 1948a, 1948b). Now, the CMB is providing the precision necessary to make accurate predictions of the light-element abundances in SBBN. In the standard model with $N_\nu = 3$, BBN makes relatively accurate predictions of the light-element abundance as displayed by the thickness of the bands in Fig. 1. These can be compared directly (or convoluted through a likelihood function) to the observational determination of the light-element abundances. The agreement between the theoretical predictions and the abundance D/H is stunning. Recent developments in the determination of D/H has produced unparalleled accuracy (Cooke *et al.*, 2014). This agreement is seen instantly when comparing the likelihood functions of the observations with those of the predictions of BBN using CMB data as seen in the second panel of Fig. 3. The helium data have also seen considerable progress. New data utilizing a near infrared emission line (Izotov, Thuan, and Guseva, 2014) have led to a marked drop in the uncertainty of the extrapolated primordial ^{4}He abundance (Aver, Olive, and Skillman, 2015). While the error remains large compared with the precision of the BBN prediction, the agreement between theory and observation is still impressive.

Is two out of three okay? Despite the success of the BBN predictions for ^{4}He and D/H, there remains a problem with ^{7}Li (Cyburt, Fields, and Olive, 2008; Fields, 2011). The predicted primordial abundance is about a factor of 3 higher than the abundance determined from absorption lines seen in a population of low-metallicity halo stars. The primordial abundance has since 1981 been associated with a narrow plateau (Spite and Spite, 1982) of abundance measurements. Recently, the extent of this plateau has been called into question as a significant amount of downward dispersion is seen at very low metallicity ($[\mathrm{Fe/H}] < -3$) (Aoki *et al.*, 2009; Sbordone *et al.*, 2010). If stellar depletion is the explanation of the discrepancy between the plateau value and the BBN prediction, it remains to be explained why there are virtually no low-metallicity stars with abundances above the plateau for all metallicities below $[\mathrm{Fe/H}] < -1.5$. If depletion is not the answer, then perhaps the lithium discrepancy points to new physics beyond the standard model.

In this review, we presented the latest combined analysis of BBN predictions using raw CMB data provided by *Planck* (Ade *et al.*, 2015; Planck Collaboration, 2015). We constructed a series of likelihood functions which include various combinations of the CMB, the BBN relation between the baryon density and the helium abundance, and various combinations of ^{4}He and D/H data. We presented detailed fits and sensitivities of the light-element abundances to the various input parameters as well as the dominant input nuclear rates. This allowed us to make relatively precise comparisons between theory and observations in standard BBN. The uncertainty in the prediction of ^{4}He remains dominated by the uncertainty in the neutron mean life. We also considered a one-parameter extension of SBBN, allowing the number of relativistic degrees of freedom characterized by the number of neutrino flavors to differ from the standard model value of $N_\nu = 3$. Despite the additional freedom, strong constraints on η and N_ν were derived. When all abundance data are used in conjunction with BBN and CMB data, we obtain a 95% C.L. upper limit of $N_\nu < 3.2$. As one of the deepest probes in big bang cosmology, BBN continues to thrive.

Going beyond 2015, we expect further improvements in the data which will better test the standard model. More high resolution data on ^{4}He emission lines could yield a further drop in the uncertainty in primordial helium. One should recall that there are still only a little over a dozen objects which are well described by models of the emission line regions. That said, there are less than half a dozen quasar absorption systems which yield high precision D/H abundances. Moreover, the nuclear physics uncertainties in D/H now dominate the error budget. Thus there is strong motivation for future measurements of the rates most important for deuterium: $d(p,\gamma)^3$He, as well as $d(d,n)^3$He, $d(d,n)t$, and $n(p,\gamma)$D (Nollett and Holder, 2011; Di Valentino *et al.*, 2014). We can hope that future measurements lead to a reduction in the already small uncertainty in primordial D/H; futuristically, there is hope of detecting cosmological 92 cm deuterium hyperfine lines that would probe D/H at extremely high redshift (Sigurdson and Furlanetto, 2006). Last, we can be certain to expect updated results from the CMB data when the *Planck* Collaboration produces its final data release.

ACKNOWLEDGMENTS

It is a pleasure to thank our recent BBN collaborators Nachiketa Chakrabory, John Ellis, Doug Friedel, Athol Kemball, Lloyd Knox, Feng Luo, Marius Millea, Tijana Prodanović, Vassilis Spanos, and Gary Steigman. The work of R. H. C. was supported by the National Science Foundation under Grant No. PHY-1430152 (JINA Center for the Evolution of the Elements). The work of K. A. O. was supported in part by DOE Grant No. DE-SC0011842 at the University of Minnesota. The work of B. D. F. and T. H. Y. was partially supported by the National Science Foundation Grant No. PHY-1214082.

APPENDIX

To use the CMB MCMC chains for BBN, it is convenient to find fitting functions for the likelihoods that the chains realize. The CMB likelihoods of interest are the 1D $\mathcal{L}(\eta)$, which is the nearly Gaussian, and 3D $\mathcal{L}(\eta, Y_p, N_{\mathrm{eff}})$, which is close to a correlated Gaussian. In order to fully capture the likelihoods, we need to include higher-order (skewness and kurtosis) terms in the multidimensional expansion.

Because the likelihoods are close to Gaussian, it is natural to describe them in an expansion using Hermite polynomials

as a basis. For parameter x with mean μ and standard deviation σ, put $z=(x-\mu)/\sigma$. In 1D, this expansion looks like

$$\mathcal{L}(x)=\frac{\exp\{-(1/2)z^2\}}{\sqrt{2\pi}\sigma}\sum c_n H_n(z) \approx \frac{\exp\{-(1/2)z^2\}}{\sqrt{2\pi}\sigma}[1+SH_3(z)+KH_4(z)]. \quad \text{(A1)}$$

Here H_n is the Hermite polynomial of degree n. The coefficients are $c_n=\langle H_n\rangle/n!=\int \mathcal{L}(x)H_n(x)dx\approx N^{-1}\sum_{\text{ichain}}^{N} H(z_i)$. Since $H_1(z)=z$ and $H_2(z)=z^2-1$, then $c_1=0$ and $c_2=0$. We find that inclusion of skewness $S\equiv c_3$ and kurtosis $K\equiv c_4$ is adequate to describe the likelihood distributions.

In multiple dimensions, the simple Gaussian base distribution is replaced with the fully correlated multidimensional Gaussian:

$$\mathcal{L}(\vec{x})=\frac{\exp\{-(1/2)(\vec{x}-\vec{\mu})^T\mathcal{C}^{-1}(\vec{x}-\vec{\mu})\}}{\sqrt{(2\pi)^d \mathrm{Det}(\mathcal{C})}} \times\Bigg[1+\sum_{n,m,p=0}^{3} S_{nmp,ijk}H_n(z_i)H_m(z_j)H_p(z_k)\delta_{3,n+m+p} + \sum_{n,m,p,q=0}^{4} K_{nmpq,ijkl}H_n(z_i)H_m(z_j) \times H_p(z_k)H_q(z_l)\delta_{4,n+m+p+q}\Bigg]. \quad \text{(A2)}$$

REFERENCES

Accetta, F. S., L. M. Krauss, and P. Romanelli, 1990, Phys. Lett. B **248**, 146.

Adams, T. F., 1976, Astron. Astrophys. **50**, 461 [http://adsabs.harvard.edu/abs/1976A%26A....50..461A].

Ade, P. A. R., *et al.* (Planck Collaboration), 2014, Astron. Astrophys. **571**, A16.

Ade, P. A. R., *et al.* (Planck Collaboration), 2015, arXiv:1502.01589.

Alpher, R., and R. Herman, 1948, Phys. Rev. **74**, 1737.

Alpher, R. A., H. Bethe, and G. Gamow, 1948, Phys. Rev. **73**, 803.

Ando, S., R. H. Cyburt, S. W. Hong, and C. H. Hyun, 2006, Phys. Rev. C **74**, 025809.

Angulo, C., *et al.*, 1999, Nucl. Phys. **A656**, 3.

Aoki, W., P. S. Barklem, T. C. Beers, N. Christlieb, S. Inoue, A. E. G. Perez, J. E. Norris, and D. Carollo, 2009, Astrophys. J. **698**, 1803.

Asplund, M., D. L. Lambert, P. E. Nissen, F. Primas, and V. V. Smith, 2006, Astrophys. J. **644**, 229.

Audouze, J., and B. M. Tinsley, 1974, Astrophys. J. **192**, 487.

Aver, E., K. A. Olive, R. L. Porter, and E. D. Skillman, **2013**, J. Cosmol. Astropart. Phys. 11, 017.

Aver, E., K. A. Olive, and E. D. Skillman, 2010, J. Cosmol. Astropart. Phys. 05, 003.

Aver, E., K. A. Olive, and E. D. Skillman, 2011, J. Cosmol. Astropart. Phys. 03, 043.

Aver, E., K. A. Olive, and E. D. Skillman, 2012, J. Cosmol. Astropart. Phys. 04, 004.

Aver, E., K. A. Olive, and E. D. Skillman, 2015, arXiv:1503.08146.

Bania, T. M., R. T. Rood, and D. S. Bania, 2002, Nature (London) **415**, 54.

Berengut, J. C., V. V. Flambaum, and V. F. Dmitriev, 2010, Phys. Lett. B **683**, 114.

Bernstein, J., L. S. Brown, and G. Feinberg, 1989, Rev. Mod. Phys. **61**, 25.

Bondarenko, L. N., V. V. Kurguzov, Yu. A. Prokofev, E. V. Rogov, and P. E. Spivak, 1978, Pis'ma Zh. Eksp. Teor. Fiz. **28**, 328 [JETP Lett. **28**, 303 (1978)].

Bonifacio, P., and P. Molaro, 1997, Mon. Not. R. Astron. Soc. **285**, 847.

Bonifacio, P., *et al.*, 2007, Astron. Astrophys. **462**, 851.

Bowman, J. D., *et al.*, 2014, arXiv:1410.5311.

Boyd, R. N., C. R. Brune, G. M. Fuller, and C. J. Smith, 2010, Phys. Rev. D **82**, 105005.

Broggini, C., L. Canton, G. Fiorentini, and F. L. Villante, **2012**, J. Cosmol. Astropart. Phys. 06, 030.

Brown, T. A. D., *et al.*, 2007, Phys. Rev. C **76**, 055801.

Burles, S., K. M. Nollett, J. W. Truran, and M. S. Turner, 1999, Phys. Rev. Lett. **82**, 4176.

Burles, S., K. M. Nollett, and M. S. Turner, 2001, Astrophys. J. **552**, L1.

Burles, S., and D. Tytler, 1998a, Astrophys. J. **499**, 699.

Burles, S., and D. Tytler, 1998b, Astrophys. J. **507**, 732.

Byrne, J., J. Morse, K. F. Smith, F. Shaikh, K. Green, and G. L. Greene, 1980, Phys. Lett. **92B**, 274.

Cameron, A. G. W., and W. A. Fowler, 1971 Astrophys. J. **164**, 111.

Casse, M., K. A. Olive, E. Vangioni-Flam, and J. Audouze, 1998, New Astron. **3**, 259.

Cayrel, R., *et al.*, 2007, Astron. Astrophys. **473**, L37.

Chakraborty, N., B. D. Fields, and K. A. Olive, 2011, Phys. Rev. D **83**, 063006.

Christensen, C. J., A. Nielsen, A. Bahnsen, W. K. Brown, and B. M. Rustad, 1972, Phys. Rev. D **5**, 1628.

Coc, A., P. Descouvemont, K. A. Olive, J.-P. Uzan, and E. Vangioni, 2012, Phys. Rev. D **86**, 043529.

Coc, A., S. Goriely, Y. Xu, M. Saimpert, and E. Vangioni, 2012, Astrophys. J. **744**, 158.

Coc, A., N. J. Nunes, K. A. Olive, J. P. Uzan, and E. Vangioni, 2007, Phys. Rev. D **76**, 023511.

Coc, A., M. Pospelov, J. P. Uzan, and E. Vangioni, 2014, Phys. Rev. D **90**, 085018.

Coc, A., J. P. Uzan, and E. Vangioni, **2014**, J. Cosmol. Astropart. Phys. 10, 050.

Coc, A., E. Vangioni-Flam, M. Cassé, and M. Rabiet, 2002, Phys. Rev. D **65**, 043510.

Coc, A., E. Vangioni-Flam, P. Descouvemont, A. Adahchour, and C. Angulo, 2004, Astrophys. J. **600**, 544.

Confortola, F., *et al.*, 2007, Phys. Rev. C **75**, 065803.

Cooke, R., M. Pettini, R. A. Jorgenson, M. T. Murphy, and C. C. Steidel, 2014, Astrophys. J. **781**, 31.

Copi, C. J., A. N. Davis, and L. M. Krauss, 2004, Phys. Rev. Lett. **92**, 171301.

Copi, C. J., D. N. Schramm, and M. S. Turner, 1997, Phys. Rev. D **55**, 3389.

Cuoco, A., F. Iocco, G. Mangano, G. Miele, O. Pisanti, and P. D. Serpico, 2004, Int. J. Mod. Phys. A **19**, 4431.

Cyburt, R. H., 2004, Phys. Rev. D **70**, 023505.

Cyburt, R. H., and B. Davids, 2008, Phys. Rev. C **78**, 064614.

Cyburt, R. H., J. Ellis, B. D. Fields, F. Luo, K. A. Olive, and V. C. Spanos, **2010**, J. Cosmol. Astropart. Phys. 10, 032.

Cyburt, R. H., J. Ellis, B. D. Fields, F. Luo, K. A. Olive, and V. C. Spanos, 2012, J. Cosmol. Astropart. Phys. 12, 037.

Cyburt, R. H., J. Ellis, B. D. Fields, F. Luo, K. A. Olive, and V. C. Spanos, 2013, J. Cosmol. Astropart. Phys. 05, 014.
Cyburt, R. H., B. D. Fields, and K. A. Olive, 2001, New Astron. **6**, 215.
Cyburt, R. H., B. D. Fields, and K. A. Olive, 2002, Astropart. Phys. **17**, 87.
Cyburt, R. H., B. D. Fields, and K. A. Olive, 2003, Phys. Lett. B **567**, 227.
Cyburt, R. H., B. D. Fields, and K. A. Olive, 2004, Phys. Rev. D **69**, 123519.
Cyburt, R. H., B. D. Fields, and K. A. Olive, **2008**, J. Cosmol. Astropart. Phys. 11, 012.
Cyburt, R. H., B. D. Fields, K. A. Olive, and E. Skillman, 2005, Astropart. Phys. **23**, 313.
Cyburt, R. H., and M. Pospelov, 2012, Int. J. Mod. Phys. E **21**, 1250004.
Dearborn, D. S. P., G. Steigman, and M. Tosi, 1996, Astrophys. J. **465**, 887.
Descouvemont, P., A. Adahchour, C. Angulo, A. Coc, and E. Vangioni-Flam, 2004, At. Data Nucl. Data Tables **88**, 203.
Dicus, D. A., E. W. Kolb, A. M. Gleeson, E. C. G. Sudarshan, V. L. Teplitz, and M. S. Turner, 1982, Phys. Rev. D **26**, 2694.
Di Valentino, E., C. Gustavino, J. Lesgourgues, G. Mangano, A. Melchiorri, G. Miele, and O. Pisanti, 2014, Phys. Rev. D **90**, 023543.
Dmitriev, V. F., V. V. Flambaum, and J. K. Webb, 2004, Phys. Rev. D **69**, 063506.
Edmunds, M. G., 1994, Mon. Not. R. Astron. Soc. **270**, L37.
Ellis, J. R., K. A. Olive, and E. Vangioni, 2005, Phys. Lett. B **619**, 30.
Epstein, R. I., J. M. Lattimer, and D. N. Schramm, 1976, Nature (London) **263**, 198.
Erken, O., P. Sikivie, H. Tam, and Q. Yang, 2012, Phys. Rev. Lett. **108**, 061304.
Fields, B. D., 1996, Astrophys. J. **456**, 478.
Fields, B. D., 2011, Annu. Rev. Nucl. Part. Sci. **61**, 47.
Fields, B. D., K. Kainulainen, K. A. Olive, and D. Thomas, 1996, New Astron. **1**, 77.
Fields, B. D., P. Molaro, and S. Sarkar, 2014, in K. A. Olive and Particle Data Group, Chin. Phys. C **38**, 339 [http://arxiv.org/abs/1412.1408v1].
Fields, B. D., and K. A. Olive, 1996, Phys. Lett. B **368**, 103.
Fields, B. D., and K. A. Olive, 1999a, Astrophys. J. **516**, 797.
Fields, B. D., and K. A. Olive, 1999b, New Astron. **4**, 255.
Fields, B. D., and K. A. Olive, 2006, Nucl. Phys. **A777**, 208.
Fields, B. D., K. A. Olive, J. Silk, M. Casse, and E. Vangioni-Flam, 2001, Astrophys. J. **563**, 653.
Fiorentini, G., E. Lisi, S. Sarkar, and F. L. Villante, 1998, Phys. Rev. D **58**, 063506.
Frebel, A., and John E. Norris, 2015, arXiv:1501.06921.
Friedel, D. N., A. Kemball, and B. D. Fields, 2011, Astrophys. J. **738**, 37.
Fumagalli, M., J. M. O'Meara, and J. X. Prochaska, 2011, Science **334**, 1245.
Galli, D., F. Palla, F. Ferrini, and U. Penco, 1995, Astrophys. J. **443**, 536.
Galli, D., L. Stanghellini, M. Tosi, and F. Palla, 1997, Astrophys. J. **477**, 218.
Gamow, G., 1948a, Phys. Rev. **74**, 505.
Gamow, G., 1948b, Nature (London) **162**, 680.
García Peréz, A. E., S. Inoue, W. Aoki, and S. G. Ryan, 2008, in *Precision Spectroscopy in Astrophysics, Proceedings of the ESO/Lisbon/Aveiro Conference* (Springer, Berlin), p. 9 [http://dx.doi.org/10.1007/978-3-540-75485-5_2].
Gott, III, J. R., J. E. Gunn, D. N. Schramm, and B. M. Tinsley, 1974, Astrophys. J. **194**, 543.
Gyürky, G., *et al.*, 2007, Phys. Rev. C **75**, 035805.
Hammache, F., *et al.*, 2013, Phys. Rev. C **88**, 062802.
Hata, N., R. J. Scherrer, G. Steigman, D. Thomas, and T. P. Walker, 1996, Astrophys. J. **458**, 637.
Heger, A., E. Kolbe, W. C. Haxton, K. Langanke, G. Martinez-Pinedo, and S. E. Woosley, 2005, Phys. Lett. B **606**, 258.
Hinshaw, G., *et al.* (WMAP Collaboration), 2013, Astrophys. J. Suppl. Ser. **208**, 19.
Hosford, A., A. E. G. Perez, R. Collet, S. G. Ryan, J. E. Norris, and K. A. Olive, 2009, Astron. Astrophys. **493**, 601.
Hosford, A., S. G. Ryan, A. E. G. Perez, J. E. Norris, and K. A. Olive, 2010, Astron. Astrophys. **511**, A47.
Hou, Z., R. Keisler, L. Knox, M. Millea, and C. Reichardt, 2013, Phys. Rev. D **87**, 083008.
Howk, J. C., N. Lehner, B. D. Fields, and G. J. Mathews, 2012, Nature (London) **489**, 121.
Hoyle, F., 1954, Astrophys. J. Suppl. Ser. **1**, 121.
Hu, W., and S. Dodelson, 2002, Annu. Rev. Astron. Astrophys. **40**, 171.
Iocco, F., G. Mangano, G. Miele, O. Pisanti, and P. D. Serpico, 2007, Phys. Rev. D **75**, 087304.
Iocco, F., G. Mangano, G. Miele, O. Pisanti, and P. D. Serpico, 2009, Phys. Rep. **472**, 1.
Izotov, Y. I., G. Stasinska, and N. G. Guseva, 2013, Astron. Astrophys. **558**, A57.
Izotov, Y. I., T. X. Thuan, and N. G. Guseva, 2014, Mon. Not. R. Astron. Soc. **445**, 778.
Izotov, Y. I., T. X. Thuan, and V. A. Lipovetsky, 1994, Astrophys. J. **435**, 647.
Izotov, Y. I., T. X. Thuan, and V. A. Lipovetsky, 1997, Astrophys. J. Suppl. Ser. **108**, 1.
Izotov, Y. I., T. X. Thuan, and G. Stasińska, 2007, Astrophys. J. **662**, 15.
Izzo, L., *et al.*, 2015, Astrophys. J. **808**, L14.
Jedamzik, K., 2004a, Phys. Rev. D **70**, 063524.
Jedamzik, K., 2004b, Phys. Rev. D **70**, 083510.
Jedamzik, K., and M. Pospelov, 2009, New J. Phys. **11**, 105028.
Kawasaki, M., K. Kohri, and T. Moroi, 2005a, Phys. Lett. B **625**, 7.
Kawasaki, M., K. Kohri, and T. Moroi, 2005b, Phys. Rev. D **71**, 083502.
Keisler, R., *et al.*, 2011, Astrophys. J. **743**, 28.
Kernan, P. J., 1993, Report No. UMI-94-01290.
Kernan, P. J., and L. M. Krauss, 1994, Phys. Rev. Lett. **72**, 3309.
Khatri, R., and R. A. Sunyaev, 2011, Astron. Lett. **37**, 367.
King, J. R., C. P. Deliyannis, and A. M. Boesgaard, 1996, Astron. J. **112**, 2839.
Kirkman, D., D. Tytler, N. Suzuki, J. M. O'Meara, and D. Lubin, 2003, Astrophys. J. Suppl. Ser. **149**, 1.
Kirsebom, O. S., and B. Davids, 2011, Phys. Rev. C **84**, 058801.
Komatsu, E., *et al.* (WMAP Science Team Collaboration), 2014, Prog. Theor. Exp. Phys. **2014**, 06B102.
Korn, A. J., *et al.*, 2006, Nature (London) **442**, 657.
Krauss, L. M., and P. J. Kernan, 1995 Phys. Lett. B **347**, 347.
Krauss, L. M., and P. Romanelli, 1990, Astrophys. J. **358**, 47.
Kusakabe, M., A. B. Balantekin, T. Kajino, and Y. Pehlivan, 2013, Phys. Lett. B **718**, 704.
Kusakabe, M., M. K. Cheoun, and K. S. Kim, 2014, Phys. Rev. D **90**, 045009.
Kusakabe, M., and M. Kawasaki, 2015, Mon. Not. R. Astron. Soc. **446**, 1597.

Levshakov, S. A., M. Dessauges-Zavadsky, S. D'Odorico, and P. Molaro, 2002, Astrophys. J. **565**, 696.
Lind, K., J. Melendez, M. Asplund, R. Collet, and Z. Magic, 2013, Astron. Astrophys. **554**, A96.
Linsky, J. L., 2003, Space Sci. Rev. **106**, 49.
Linsky, J. L., *et al.*, 2006, Astrophys. J. **647**, 1106.
Lisi, E., S. Sarkar, and F. L. Villante, 1999, Phys. Rev. D **59**, 123520.
Lopez, R. E., M. S. Turner, and G. Gyuk, 1997, Phys. Rev. D **56**, 3191.
Mampe, W., P. Ageron, C. Bates, J. M. Pendlebury, and A. Steyerl, 1989, Phys. Rev. Lett. **63**, 593.
Mangano, G., and P. D. Serpico, 2011, Phys. Lett. B **701**, 296.
Mathews, G. J., T. Kajino, and T. Shima, 2005, Phys. Rev. D **71**, 021302.
Melendez, J., and I. Ramirez, 2004, Astrophys. J. **615**, L33.
Meneguzzi, M., J. Audouze, and H. Reeves, 1971, Astron. Astrophys. **15**, 337 [http://adsabs.harvard.edu/abs/1971A%26A....15..337M].
Molaro, P., F. Primas, and P. Bonifacio, 1995, Astron. Astrophys. **295**, L47 [http://adsabs.harvard.edu/abs/1995A%26A...295L..47M].
Moos, H. W., *et al.*, 2002, Astrophys. J. Suppl. Ser. **140**, 3.
Mukhanov, V., 2005, *Physical Foundations of Cosmology* (Cambridge University Press, Cambridge, UK), p. 421.
Mukhanov, V. F., 2004, Int. J. Theor. Phys. **43**, 669.
Nollett, K. M., and S. Burles, 2000, Phys. Rev. D **61**, 123505.
Nollett, K. M., and G. P. Holder, 2011, arXiv:1112.2683.
Noterdaeme, P., S. Lopez, V. Dumont, C. Ledoux, P. Molaro, and P. Petitjean, 2012, Astron. Astrophys. **542**, L33.
Olive, K. A., P. Petitjean, E. Vangioni, and J. Silk, 2012, Mon. Not. R. Astron. Soc. **426**, 1427.
Olive, K. A., N. Prantzos, S. Scully, and E. Vangioni-Flam, 1994, Astrophys. J. **424**, 666.
Olive, K. A., R. T. Rood, D. N. Schramm, J. W. Truran, and E. Vangioni-Flam, 1995, Astrophys. J. **444**, 680.
Olive, K. A., D. N. Schramm, S. T. Scully, and J. W. Truran, 1997, Astrophys. J. **479**, 752.
Olive, K. A., D. N. Schramm, G. Steigman, M. S. Turner, and J.-M. Yang, 1981, Astrophys. J. **246**, 557.
Olive, K. A., D. N. Schramm, G. Steigman, and T. P. Walker, 1990, Phys. Lett. B **236**, 454.
Olive, K. A., and E. D. Skillman, 2001, New Astron. **6**, 119.
Olive, K. A., and E. D. Skillman, 2004, Astrophys. J. **617**, 29.
Olive, K. A., and G. Steigman, 1995, Phys. Lett. B **354**, 357.
Olive, K. A., G. Steigman, and T. P. Walker, 2000, Phys. Rep. **333–334**, 389.
Olive, K. A., and D. Thomas, 1997, Astropart. Phys. **7**, 27.
Olive, K. A., and D. Thomas, 1999, Astropart. Phys. **11**, 403.
Olive, K. A., *et al.* (Particle Data Group Collaboration), 2014, Chin. Phys. C **38**, 090001.
O'Malley, P. D., *et al.*, 2011, Phys. Rev. C **84**, 042801.
O'Meara, J. M., S. Burles, J. X. Prochaska, G. E. Prochter, R. A. Bernstein, and K. M. Burgess, 2006, Astrophys. J. **649**, L61.
O'Meara, J. M., D. Tytler, D. Kirkman, N. Suzuki, J. X. Prochaska, D. Lubin, and A. M. Wolfe, 2001, Astrophys. J. **552**, 718.
Ostriker, J. P., and B. M. Tinsley, 1975, Astrophys. J. **201**, L51.
Paris, M. W., G. M. Hale, A. C. Hayes-Sterbenz, and G. Jungman, 2013, arXiv:1304.3153.
Peimbert, M., V. Luridiana, and A. Peimbert, 2007, Astrophys. J. **666**, 636.
Peimbert, M., and S. Torres-Peimbert, 1974, Astrophys. J. **193**, 327.
Perez, A. E. G., W. Aoki, S. Inoue, S. G. Ryan, T. K. Suzuki, and M. Chiba, 2009, Astron. Astrophys. **504**, 213.
Pettini, M., and D. V. Bowen, 2001, Astrophys. J. **560**, 41.
Pettini, M., and R. Cooke, 2012, Mon. Not. R. Astron. Soc. **425**, 2477.
Pettini, M., B. J. Zych, M. T. Murphy, A. Lewis, and C. C. Steidel, 2008, Mon. Not. R. Astron. Soc. **391**, 1499.
Pinsonneault, M. H., G. Steigman, T. P. Walker, and V. K. Narayanan, 2002, Astrophys. J. **574**, 398.
Pinsonneault, M. H., T. P. Walker, G. Steigman, and V. K. Narayanan, 1999, Astrophys. J. **527**, 180.
Pisanti, O., A. Cirillo, S. Esposito, F. Iocco, G. Mangano, G. Miele, and P. D. Serpico, 2008, Comput. Phys. Commun. **178**, 956.
Planck Collaboration, 2015, taken from the download of the Full Grid of Cosmological Parameters found at http://irsa.ipac.caltech.edu/data/Planck/release_2/ancillary-data/.
Porter, R. L., G. J. Ferland, P. J. Storey, and M. J. Detisch, 2012, Mon. Not. R. Astron. Soc. **425**, L28.
Porter, R. L., G. J. Ferland, P. J. Storey, and M. J. Detisch, 2013, Mon. Not. R. Astron. Soc. **433**, L89.
Pospelov, M., and N. Afshordi, 2012, arXiv:1208.0793.
Pospelov, M., and J. Pradler, 2010, Annu. Rev. Nucl. Part. Sci. **60**, 539.
Poulin, V., and P. D. Serpico, 2015, Phys. Rev. Lett. **114**, 091101.
Prantzos, N., M. Cassé, and E. Vangioni-Flam, 1993, Astrophys. J. **403**, 630.
Prodanović, T., and B. D. Fields, 2003, Astrophys. J. **597**, 48.
Prodanović, T., G. Steigman, and B. D. Fields, 2010, Mon. Not. R. Astron. Soc. **406**, 1108.
Ramaty, R., B. Kozlovsky, R. Lingenfelter, and H. Reeves, 1997, Astrophys. J. **488**, 730.
Reeves, H., J. Audouze, W. A. Fowler, and D. N. Schramm, 1973, Astrophys. J. **179**, 909.
Reeves, H., W. A. Fowler, and F. Hoyle, 1970, Nature (London) **226**, 727.
Reimer-Sørensen, S., *et al.*, 2015, Mon. Not. R. Astron. Soc. **447**, 2925.
Richard, O., G. Michaud, and J. Richer, 2005, Astrophys. J. **619**, 538.
Rollinde, E., E. Vangioni-Flam, and K. A. Olive, 2005, Astrophys. J. **627**, 666.
Rood, R. T., T. L. Wilson, and G. Steigman, 1979, Astrophys. J. **227**, L97.
Ryan, S. G., T. C. Beers, K. A. Olive, B. D. Fields, and J. E. Norris, 2000, Astrophys. J. **530**, L57.
Ryan, S. G., J. E. Norris, and T. C. Beers, 1999, Astrophys. J. **523**, 654.
Sarkar, S., 1996, Rep. Prog. Phys. **59**, 1493.
Savage, B., N. Lehner, A. Fox, B. Wakker, and K. Sembach, 2007, Astrophys. J. **659**, 1222.
Sbordone, L., *et al.*, 2010, Astron. Astrophys. **522**, A26.
Scully, S., M. Casse, K. A. Olive, and E. Vangioni-Flam, 1997, Astrophys. J. **476**, 521.
Scully, S. T., M. Casse, K. A. Olive, D. N. Schramm, J. Truran, and E. Vangioni-Flam, 1996, Astrophys. J. **462**, 960.
Seckel, D., 1993, arXiv:hep-ph/9305311.
Serebrov, A., *et al.*, 2005, Phys. Lett. B **605**, 72.
Serpico, P. D., S. Esposito, F. Iocco, G. Mangano, G. Miele, and O. Pisanti, **2004**, J. Cosmol. Astropart. Phys. 12, 010.
Shvartsman, V. F., 1969, Pisma Zh. Eksp. Teor. Fiz. **9**, 315 [JETP Lett. **9**, 184 (1969)].
Sievers, J. L., *et al.* (Atacama Cosmology Telescope Collaboration), **2013**, J. Cosmol. Astropart. Phys. 10, 060.

Sigurdson, K., and S. R. Furlanetto, 2006, Phys. Rev. Lett. **97**, 091301.
Singh, B. S. N., *et al.*, 2004, Phys. Rev. Lett. **93**, 262503.
Smith, C. J., and G. M. Fuller, 2010, Phys. Rev. D **81**, 065027.
Smith, M. S., L. H. Kawano, and R. A. Malaney, 1993, Astrophys. J. Suppl. Ser. **85**, 219.
Spergel, D. N., *et al.* (WMAP Collaboration), 2003, Astrophys. J. Suppl. Ser. **148**, 175.
Spite, F., and M. Spite, 1982, Astron. Astrophys. **115**, 357.
Srianand, R., N. Gupta, P. Petitjean, P. Noterdaeme, and C. Ledoux, 2010, Mon. Not. R. Astron. Soc. **405**, 1888.
Steffen, M., R. Cayrel, P. Bonifacio, H. G. Ludwig, and E. Caffau, 2009, IAU Symp., **5**, 23.
Steigman, G., **2006**, J. Cosmol. Astropart. Phys. 10, 016.
Steigman, G., 2007, Annu. Rev. Nucl. Part. Sci. **57**, 463.
Steigman, G., K. A. Olive, D. N. Schramm, and M. S. Turner, 1986, Phys. Lett. B **176**, 33.
Steigman, G., D. Romano, and M. Tosi, 2007, Mon. Not. R. Astron. Soc. **378**, 576.
Steigman, G., D. N. Schramm, and J. E. Gunn, 1977 Phys. Lett. B **66**, 202.
Steigman, G., and M. Tosi, 1992, Astrophys. J. **401**, 150.
Switzer, E. R., and C. M. Hirata, 2005, Phys. Rev. D **72**, 083002.
Tajitsu, A., K. Sadakane, H. Naito, A. Arai, and W. Aoki, 2015, Nature (London) **518**, 381.
Tosi, M., G. Steigman, F. Matteucci, and C. Chiappini, 1998, Astrophys. J. **498**, 226.
Vangioni, E., J. Silk, K. A. Olive, and B. D. Fields, 2011, Mon. Not. R. Astron. Soc. **413**, 2987.
Vangioni-Flam, E., and J. Audouze, 1988, Astron. Astrophys. **193**, 81 [http://adsabs.harvard.edu/abs/1988A%26A...193...81V].
Vangioni-Flam, E., M. Casse, R. Cayrel, J. Audouze, M. Spite, and F. Spite, 1999, New Astron. **4**, 245.
Vangioni-Flam, E., A. Coc, and M. Casse, 2000, Astron. Astrophys. **360**, 15 [http://adsabs.harvard.edu/abs/2000A%26A...360...15V].
Vangioni-Flam, E., K. A. Olive, B. D. Fields, and M. Casse, 2003, Astrophys. J. **585**, 611.
Vangioni-Flam, E., K. A. Olive, and N. Prantzos, 1994, Astrophys. J. **427**, 618.
Vauclair, S., and C. Charbonnel, 1998, Astrophys. J. **502**, 372.
Wagoner, R. V., 1969, Astrophys. J. Suppl. Ser. **18**, 247.
Walker, T. P., G. Steigman, D. N. Schramm, K. A. Olive, and H. S. Kang, 1991, Astrophys. J. **376**, 51.
Weinberg, S., 2008, *Cosmology* (Oxford University Press, Oxford, UK), p. 593.
White, M. J., D. Scott, and J. Silk, 1994, Annu. Rev. Astron. Astrophys. **32**, 319.
Wood, B. E., J. L. Linsky, G. Hebrard, G. M. Williger, H. W. Moos, and W. P. Blair, 2004, Astrophys. J. **609**, 838.
Woosley, S. E., D. H. Hartmann, R. D. Hoffman, and W. C. Haxton, 1990, Astrophys. J. **356**, 272.
Xu, Y., K. Takahashi, S. Goriely, M. Arnould, M. Ohta, and H. Utsunomiya, 2013, Nucl. Phys. **A918**, 61.
Yang, J. M., D. N. Schramm, G. Steigman, and R. T. Rood, 1979, Astrophys. J. **227**, 697.
Yang, J. M., M. S. Turner, G. Steigman, D. N. Schramm, and K. A. Olive, 1984, Astrophys. J. **281**, 493.
Yue, A. T., M. S. Dewey, D. M. Gilliam, G. L. Greene, A. B. Laptev, J. S. Nico, W. M. Snow, and F. E. Wietfeldt, 2013, Phys. Rev. Lett. **111**, 222501.